Novel Treatments For Multi-phase Flow Prediction Inspired By Kinetic Theory

by

Zakaria Ben Dhia

Thesis submitted to the
Faculty of Graduate and Postdoctoral Studies
In partial fulfillment of the requirements
For the M.A.Sc. degree in
Mechanical Engineering

School of Mechanical Engineering
Faculty of Engineering
University of Ottawa

Abstract

This study entails an investigation of a novel moment closure, originally constructed for rarefied-gas prediction, to the modelling of inert, dilute, disperse, particle flows. Such flows are important in many engineering situations. As one example, in internal-combustion engines, fuel is often injected as a spray of tiny droplets and, during combustion, a cloud of tiny soot particles can be formed. These particle phases are often difficult to model, especially when particles display a range of velocities at each location in space. Lagrangian methods are often too costly and many Eulerian field-based methods suffer from model deficiencies and mathematical artifacts. Often, Eulerian formulations assume that all particles at a location and time have the same velocity. This assumption leads to nonphysical results, including an inability to predict particle paths crossing and a limited number of boundary conditions that can be applied.

The typical multi-phase situation of many particles is, in many ways, similar to that of a gas compressed of a huge number of atoms or molecules. It is therefore expected that powerful techniques from the kinetic theory of gases could be applied. This work explores the advantages of using a modern fourteen-moment model, originally derived for rarefied gases, to predict multi-phase flows. Details regarding the derivation, the mathematical structure, and physical behaviour of the resulting model are explained. Finally, a numerical implementation is presented and results for several flow problems that are designed to demonstrate the fundamental behaviour of the models are presented. Comparisons are made with other classical models.

Acknowledgements

I wish to thank my family for their support during my studies. I am especially grateful of the support and encouragement that my parents have offered me over the years. My wife, Syrine, has always been there for me and gives her support and love for everything I have pursued during my life.

I feel privileged to have had the opportunity to continue my education at the University of Ottawa Department of Mechanical Engineering. During my program, I was lucky to work with an amazing group of professors and wonderful colleagues. I would like to thank my thesis adviser, Professor James McDonald, for his support, guidance and encouragement that made this thesis possible. He has shared his knowledge in the field of moment closure and computational fluid dynamics with me over my program and given every opportunity to take part in the research community. I am also grateful to him for his financial support.

Zakaria Ben Dhia

University of Ottawa Department of Mechanical Engineering

May 2016

Table of Contents

List of Figures

Nomenclature

A	Flux Jacobian matrix in the x direction
a_d	Acceleration of a particle
a_i	Acceleration vector
B	Flux Jacobian matrix in the y direction
c_i	Random-velocity vector
d	Particle diameter
E	Energy density
H	Entropy density
l_0	Characteristic length
$\mathcal{F}$	Distribution function
$\mathcal{M}$	Maxwell-Boltzmann distribution
m	Particle mass
N	Number of particles

P_{ij} Anisotropic pressure tensor

Q_{ijk} Generalized heat-flux tensor

R_{ijjkk} Tensor containing fourth-order random moments

S Source term

S_{ijkl} Tensor containing fifth-order random moments

St Stokes number

t Time

u_g Background velocity

u_i Bulk-velocity vector

$\mathbf{U}^k$ Vector of N conserved moments

V_0 Fluid velocity

v_i Velocity vector

W Velocity-dependent weight

x_i Position vector

α Free parameter

λ Wave speed

μ_g Dynamic viscosity

$\boldsymbol{\phi}$	Generating velocity weights
ρ_p	Material density of the particle phase
τ	Relaxation time of particle due to drag

Chapter 1

Introduction

It is plainly apparent that human activities have undesired effects on the natural environment. It is highly desirable to minimize these effects by making technology as efficient and clean as possible. For example, improved control of combustion in engines could reduce pollution generation. To accomplish this, a sophisticated understanding of the multi-phase flow occurring in the engine is necessary.

Multi-phase flows are omnipresent in numerous practical engineering situations. They are defined as the concurrent flow of materials with diverse states or phases (i.e., gas, solid, or liquid). Examples of such flows include: gas-liquid-solid flows in chemical reactors, solid-gas flows in pneumatic conveying, and gas-liquid flows in evaporators and condensers. In internal-combustion engines, fuel is often injected as a spray of tiny droplets and, during combustion, a cloud of microscopic soot particles can be formed. The design of clean and efficient combustion technologies rests on an ability to make accurate predictions and analysis of these situation.

The description of such flows involves tracking or modelling the motions of a huge number of particle trajectories. Figure 1.1 illustrates some families of common techniques used

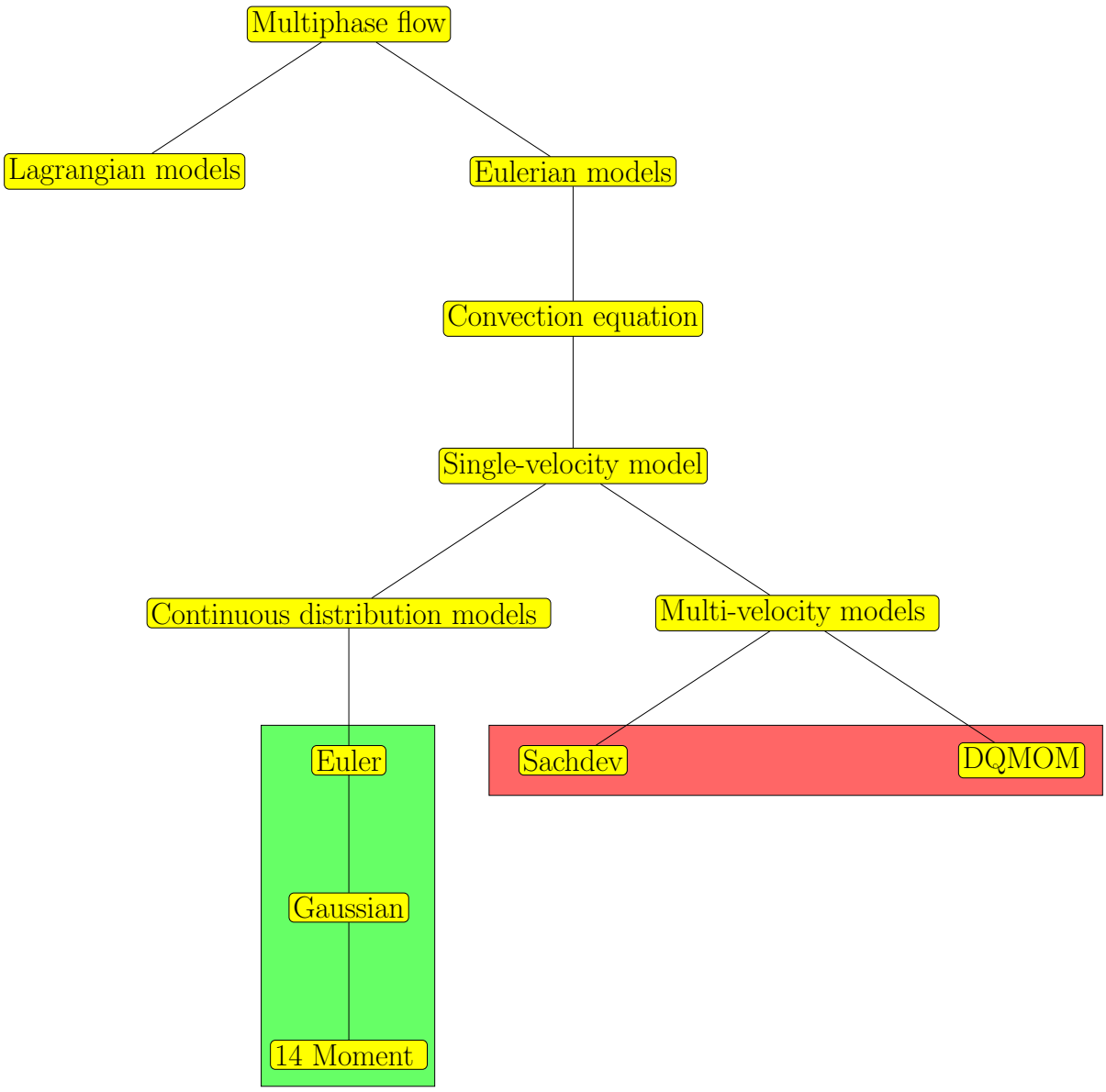

Figure 1.1: *Hierarchy of models for multi-phase flow prediction*

to model multi-phase flow. We start with the Lagrangian treatment. In this treatment, we track the evolution of individual particles through the direct integration of Newton's laws of motion for each particle. This is conceptually simple, but computationally expensive, as an immensely large number of particles are often present, even at dilute concentrations. The other family of methods are referred to as Eulerian. In these methods the particle phase is modelled as a continuum and partial differential equations (PDEs) are defined that govern the evolution of field variables with position and time as independent variables. The most basic Eulerian formulation is simply a convection equation. It restricts all particle velocities at a given position and time to be equal to that of the background fluid. This method can work well for flows in which the particle phase is very close to an equilibrium with the carrier phase. This is to say, when the particles all have a velocity that is nearly identical to the carrier phase velocity. For flows in which this assumption is not valid, a classical, single-velocity model is more flexible. It allows the particle velocity to deviate from that of the gas, but restricts all particles at a location and time to have the same velocity as each other. This classical, single-velocity model for particle flows is standard and has been widely used [28, 26]. In many applications, this is an accuracy model, especially in cases when drag forces between the gas and the particles are dominant and particles tend to all have velocities that don't deviate much from that of the gas. However, this is an invalid assumption in other cases and forcing all particles to have the same velocity leads to artifacts in the model and causes it to produce completely nonphysical predictions in some cases [28, 29]. As an example, this model cannot predict the crossing of two beams of non-interacting particles.

The physical situation of a huge number of independent, practically indistinguishable, solid particles is very similar to the situation of a gas that is comprised of an enormous number of identical atoms or molecules. It is therefore expected that the field of gaskinetic theory can be used as a guide in this situation [7]. The technique of moment closures from gaskinetic theory seems promising as a source of new models for multi-phase flows. This technique leads to an expanded set of partial differential equations that describe the evolution of statistical properties of the particle-velocity distributions. These equations are in the form of a system of first-order hyperbolic balance laws that are amenable to solution using standard numerical techniques. In general, the solution of these PDEs promise enhanced physical accuracy while requiring considerably less effort than obtaining solutions using a direct particle simulation.

Previous studies have had some success in applying techniques from kinetic theory to multi-phase flow prediction. One technique allows particles at a location to have one of a set of possible velocities. This can be accomplished by considering multi-velocity formulations in which particles are grouped into families. However, these treatments often group particles based on a predefined separation of velocity space, as was done by Sachdev [27]. All of the deficiencies of a single-velocity formulation can still be observed for cases that are selected to illustrate the artifacts. Additionally, the resulting model equations are not Galilean invariant as the segregation of velocity space is done in a fixed reference frame. For example, DQMOM model of Desjardins et al. [23] is not invariant under rotation.

Another technique is to allow particles to have a continuous range of velocities. One model in this family involves applying the compressible Euler equations to the particle

phase. This technique is commonly used and available in many multi-phase flow solvers. Another model, originally derived by Levermore and Morokoff [2, 1, 18], admits 10 equations. The 10-moment Gaussian closure model is a moment closures and allows the standard deviation of particle velocities to be different in different directions [9, 17, 22]. This model has been recently applied to particle flows by Vie et al. [30] in preliminary study. In 2013, a new moment closure of the Boltzmann equation was presented by McDonald and Torrilhon [21]. It is based on an approximation of the maximum-entropy hierarchy. This model allows the statistics describing particle velocities to be bi-model. It is expected that this will greatly improve the accuracy of the predictions for multi-phase flow. Up to now, this model has only been applied to pure gas flow. This work represents its first application to multi-phase flow prediction.

1.1 Objectives and Relevance

The objective of the current study is to investigate new moment-closure models that might alleviate the single-velocity model deficiencies and their mathematical artifacts [21]. We investigate the modelling of inert, dilute, disperse, particle flows in challenging multi-phase flow situations (e.g. particles-crossing). These particle flows are often difficult to model, especially when particles display a range of velocities at each location in space. Details regarding the derivation, the mathematical structure, and the physical behaviour of the chosen models are explained. Finally a numerical implementation is presented and results for several flow problems that are designed to demonstrate the fundamental and limitations behaviour of each model are presented. It is demonstrated that the added

physical accuracy of higher-order moment methods are Galilean invariant models which allow particle crossing. It is through that this work represents the first even demonstration of this.

1.2 Scope of Present Study

This current study reviews the derivation of several multi-velocity models for particle-laden gas flows based on kinetic theory. The physical behaviour and limitations of each model is demonstrated. Aspects of numerical implementation are presented. In Chapter 2, we begin with a review of gaskinetic theory and the mathematical properties of the maximum-entropy moment closures. Also in this chapter, we introduce practical difficulties of the use of this maximum-entropy technique. In Chapter 3, we explain the construction of several models: the single velocity model, the multi-velocity model, the Euler model and the Gaussian model. The physical behaviour and limitations of the models are discussed. In Chapter 4, we review the new fourteen-moment model [21] that was proposed for gas flow prediction and show how it is modified to model multi-phase flow. In Chapter 5, a numerical method for the solution of the resulting governing equations is presented. In Chapter 6, results of numerical computation of several different problems, solved with several models are shown. The particular cases are chosen to clearly demonstrate the fundamental behaviour and limitations of each model. Finally, the last chapter concludes with a summary of achievements and a view to future research.

1.3 Statement of Contribution

During this work, I investigate the use of a fourteen-moment closure model that might alleviate typical mathematical artifacts associated with multi-phase phenomena. For example, in the case of two or more groups of intersecting particles, crossing is impossible in common models. This work is the first application of the fourteen-moment model to such multi-phase flows. Through the use of kinetic theory of gases, traditional models are rederived for comparison to the new model. In all cases suitable acceleration terms resulting from particle drag are derived. A new computer code is constracted and used to compare all models.

Chapter 2

Overview of Multi-Phase Flows and Gaskinetic Theory

2.1 Multi-Phase Flow

The behaviours of multi-phase gas-particle flows can be characterized through the definition of the Stokes number, St, for a particle in a background flow. It is defined as the ratio of the characteristic time of a particle (or droplet) to a characteristic time of the flow [25, 31].

$$\mathrm{St} = \frac{\tau V_0}{l_0}\,, \tag{2.1}$$

where V_0 is the fluid velocity of the flow well away from a particle, l_0 is the characteristic dimension of the particle, and τ is the relaxation time of the particle due to the effect of the drag force on the particle velocity. For the current study, it is assumed that the flow around each particle is well approximated by Stokes flow. The Stokes law can model the drag between the particle and background fluid when the particle Reynolds number is low. The acceleration of a particle due to drag, $a_d(t, x, v)$, is due to the velocity difference between the particle phase and the background phase. For Stokes flow, it can be expressed

Table 2.1: Definition of several multi-phase flow regimes

$\mathrm{St} \ll 1$	Particle velocity is nearly the same as the fluid velocity
$\mathrm{St} \approx 1$	Significant velocity difference are present
$\mathrm{St} \gg 1$	Particles are very weakly influenced by the fluid

as

$$a_d(t, x, v) = \frac{\mathrm{u}_g(t, x) - v}{\tau}\,, \tag{2.2}$$

with

$$\tau = \frac{\rho_p d_p^2}{\mu_g 18}\,, \tag{2.3}$$

where u_g is the background velocity, $\mu_{\mathbf{g}}$ is the dynamic viscosity, $\rho_{\mathbf{p}}$ is the material density of the particle phase and d_p is the particle diameter. This relation follows from the assumption of Stokes flow.

The Stokes number can be used to define several regimes which characterize the importance of particles drag in flow behaviour. This separation is shown in Table 2.1. When $\mathrm{St} \ll 1$, this regime indicates that the particle motion is tightly coupled to the fluid motion. Simple models, which ensure that particles have the same velocity as the background fluid, are the best models to use for this regime. When $\mathrm{St} \approx 1$, particles are still strongly affected by the flow but can have significantly different velocities. When $\mathrm{St} \gg 1$, particles are only weakly influences by the fluid. Their response time is longer than the time the fluid has to act on it and so the particle will pass through the flow without much deflection in its initial trajectory. Traditionally, when the Stokes number becomes very large, the details of gas-particle behaviours become vital in an understanding of the situation. In such situations, traditional fluid mechanics cannot be used to accurately describe multi-phase flows behaviour. For such situations the development of new advanced methods is required to

make accurate predictions possible. In developing such models, it is thought that the field of kinetic theory of gases can serve as a guide.

2.2 Kinetic Theory of Gases

The objective of the kinetic theory is to describe the macroscopic properties of gases (i.e pressure, temperature) using classical mechanics and a statistical representation of particle velocity distributions. The multi-phase physical situation of a huge number of independent, practically indiscernible solid particles is, in many ways, similar to that of a gas composed of a huge number of atoms or molecules. It is therefore expected that powerful techniques from the kinetic theory of gases could be equally applied to multi-phase flows. Kinetic theory describes the microscopic state of a gas through the definition of a probability density functions, $\mathcal{F}(x_i, v_i, t)$. Here, $\mathcal{F}(x_i, v_i, t)$, is a function that describes the relative likelihood for a gas particle have a given position, x_i, with a velocity, v_i, at time, t. An illustration of a distribution function for a simple one-dimensional setting is shown in Figure 2.1. This distribution describes all gas particles near a given point at a given time. It can be seen that most particles have a velocity near zero, through a significant number have a velocity near negative four.

Specifically, the distribution function is defined such that

$$\mathrm{N}x_i v_i = \mathcal{F}(x_i, v_i, t)\ \mathrm{d}x_i \mathrm{d}v_i, \tag{2.4}$$

where $\mathrm{N}x_i v_i$ gives the number of particles existing in a six-dimensional phase space with velocities between the range of v_i and $v_i + \mathrm{d}v_i$ located in a space interval of x_i and $x_i + \mathrm{d}x_i$ at time t, as shown in Figure 2.2. Integrating Equation (2.4) over all possible velocities

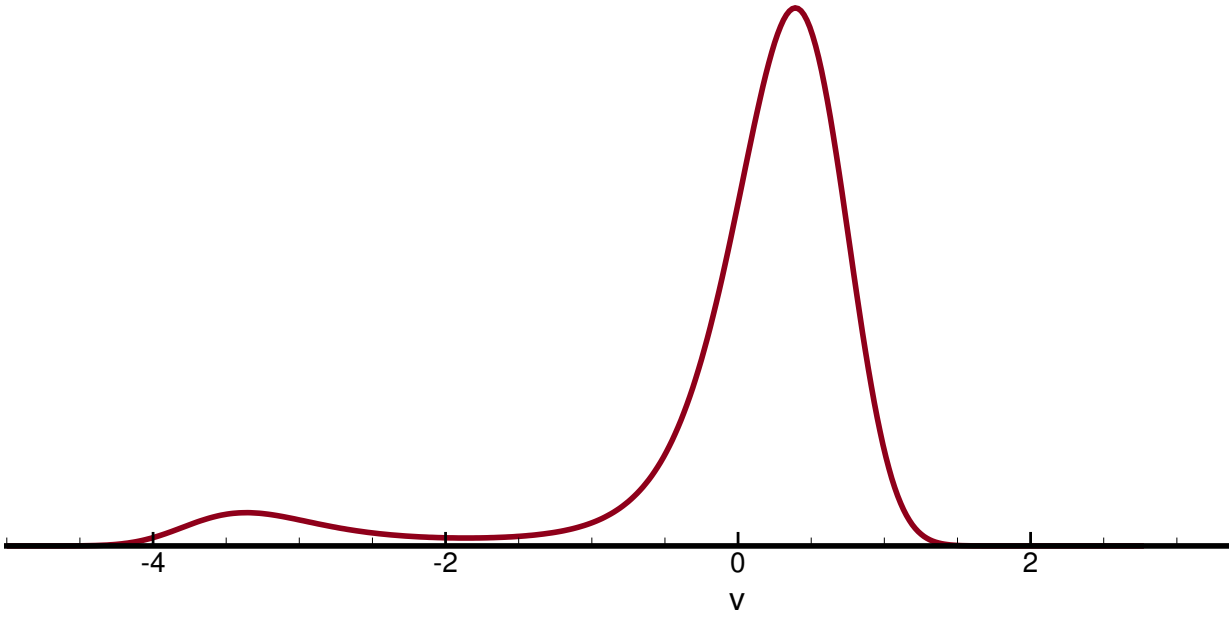

Figure 2.1: *Illustration of a typical distribution function, $\mathcal{F}(x_i, v_i, t)$, at a fixed x_i and t.*

and locations gives the total number of particles composing a gas,

$$\mathrm{N} = \int_V \int_X \mathcal{F}(x_i, v_i, t) \mathrm{d}v_i \mathrm{d}x_i \,. \tag{2.5}$$

2.2.1 The Boltzmann Equation

The Boltzmann equation describes the evolution of the probability density function, where interactions are limited to binary collisions [4, 3, 7]. This is a high-dimensional integro-differential equation for $\mathcal{F}$ having the form

$$\frac{\partial \mathcal{F}}{\partial t} + v_i \frac{\partial \mathcal{F}}{\partial x_i} + \frac{\partial a_i \mathcal{F}}{\partial v_i} = \frac{\delta \mathcal{F}}{\delta t} \,, \tag{2.6}$$

where the term on the right hand side of the equation, $\frac{\delta \mathcal{F}}{\delta t}$, is the collision integral and represents the time rate of change of the distribution function produced by inter-particle collisions. Here, a_i is the acceleration of particles due to external forces.

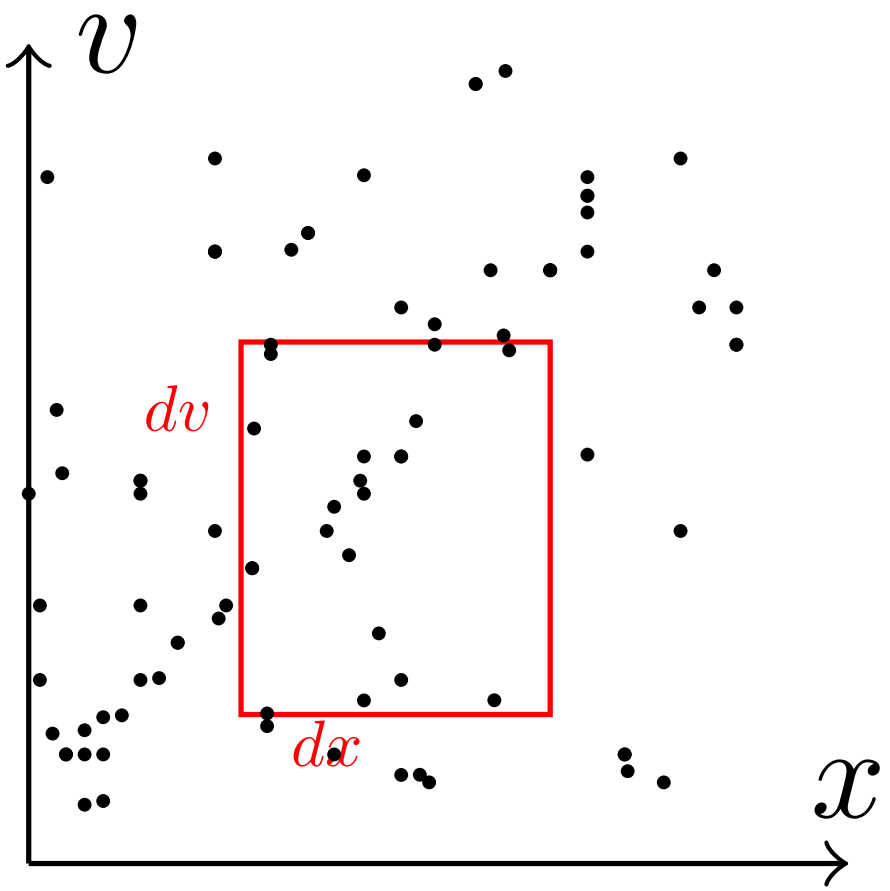

Figure 2.2: *Representation of the two-dimensional phase space and a differential cell of phase space. Each dot represents the momentary state of one gas particle.*

2.2.2 Moments of Distribution Functions

In order to relate the macroscopic properties of a gas (i.e pressure, temperature, mass density, velocity, etc) to a particular distribution function, $\mathcal{F}(x_i, v_i, t)$, velocity moments must be taken. Macroscopic properties of the gas, at a particular location and time, are obtained by taking appropriate velocity moments of $\mathcal{F}$. This is done by integrating the product of the distribution function and an appropriate velocity-dependent weight, $W(v_i)$, over all velocity space,

$$\langle W\mathcal{F}\rangle = \iiint_{\infty} W\mathcal{F}(x_i, v_i, t)d^3v\,. \tag{2.7}$$

For example, the mass density, ρ, can be determined by taking the molecular mass, m, of the gas as the weighting function,

$$\rho(x_i, t) = \iiint_{\infty} m\mathcal{F}(x_i, v_i, t)\ \mathrm{d}^3v_i = \langle m\mathcal{F}\rangle\ . \tag{2.8}$$

Here the compact notation $\langle\mathcal{F}\rangle$ is used to denote integration over all velocity space. It is possible to separate the particle velocity, v_i into two components: the bulk velocity, u_i, where $\rho u_i = \langle mv_i\mathcal{F}\rangle$, and the random velocity, c_i, such that $v_i = u_i + c_i$. Moments can also be taken using weights dependent on the random component of particle velocity, $W(c_i)$. For example, the second-order random moment of $\mathcal{F}$ is

$$P_{ij} = \langle mc_ic_j\mathcal{F}\rangle\ . \tag{2.9}$$

Here, P_{ij} is the anisotropic pressure tensor. This tensor is a combination of the traditional fluid pressure and viscous stress. It is related to the thermodynamic pressure, p, through $p = P_{ii}/3$. Similar to the pressure tensor, by integrating the product of the distribution

function $\mathcal{F}$ and an appropriate velocity-dependent weight $W(v_i)$, we define the following notation for general velocity moments of $\mathcal{F}$:

$$U_0 = \rho = \iiint_\infty m\mathcal{F}\,\mathrm{d}v_i = \langle m\mathcal{F}\rangle$$

$$U_x = \rho u_i = \langle mv_i\mathcal{F}\rangle \qquad c_i = v_i - u_i$$

$$U_{xy} = \langle mv_xv_y\mathcal{F}\rangle$$

$$U_{xii} = \langle mv_xv_iv_i\mathcal{F}\rangle$$

$$P_{ij} = \langle mc_ic_j\mathcal{F}\rangle$$

$$Q_{ijk} = \langle mc_ic_jc_k\mathcal{F}\rangle$$

$$R_{ijkl} = \langle mc_ic_jc_kc_l\mathcal{F}\rangle$$

Here, third- and fourth-order moments of the random velocity are given the symbols Q_{ijk} and R_{ijkl}. All higher-order moments of the full particle velocity, v_i, are given the symbol U. The number of times a coordinate appears in the subscript of the symbol U denotes the number of times that velocity component appears in the generating weight. Using this method, we can take the moments of arbitrarily high order, but as the order of a moment becomes higher, its physical significance becomes less clear. The Einstein summation convention is used for general indices (i, j, k, etc.), but not for specific Cartesian directions (x, y, z). For example, $v_iv_i = v_x^2 + v_y^2 + v_z^2$, but P_{xx} refers to a single early in the tensor, P_{ij}.

2.2.3 Maxwells Equation of Change

In order to determine the time evolution of the macroscopic quantity associated with a velocity weight, $W(v_i)$, we take moments of the Boltzmann equation. This gives

$$\frac{\partial}{\partial t}\langle W\mathcal{F}\rangle + \frac{\partial}{\partial x_i}\langle v_i W\mathcal{F}\rangle + \left\langle \frac{\partial}{\partial v_i} a_i W\mathcal{F}\right\rangle = \left\langle W\frac{\delta\mathcal{F}}{\delta t}\right\rangle . \tag{2.10}$$

By introducing the notation: $\Delta[W\mathcal{F}] = \left\langle W\frac{\delta\mathcal{F}}{\delta t}\right\rangle$, equation (2.10) can be re expressed as

$$\frac{\partial}{\partial t}\langle W\mathcal{F}\rangle + \frac{\partial}{\partial x_i}\langle v_i W\mathcal{F}\rangle + \left\langle \frac{\partial}{\partial v_i} a_i W\mathcal{F}\right\rangle = \Delta[W\mathcal{F}]\,. \tag{2.11}$$

This is Maxwell's equation of change written in conservative form. To define a set of moment equations describing the evolution of multiple macroscopic quantities a vector of velocity-dependent weights, $\mathbf{W}(v_i)^{(k)}$, is used in place of an individual weight. The result will be a coupled set of k moment equations describing the evolution of the corresponding conserved moments, $U^k = \left\langle \mathbf{W}^{(k)}\mathcal{F}\right\rangle$,

$$\frac{\partial}{\partial t}\left\langle \mathbf{W}^{(k)}\mathcal{F}\right\rangle + \frac{\partial}{\partial x_i}\left\langle v_i\mathbf{W}^{(k)}\mathcal{F}\right\rangle + \left\langle \frac{\partial}{\partial v_i} a_i\mathbf{W}^{(k)}\mathcal{F}\right\rangle = \Delta[\mathbf{W}^{(k)}\mathcal{F}]\,, \tag{2.12}$$

or

$$\frac{\partial\mathbf{U}^{(k)}}{\partial t} + \frac{\partial}{\partial x_i}\left\langle v_i\mathbf{W}^{(k)}\mathcal{F}\right\rangle + \left\langle \frac{\partial}{\partial v_i} a_i\mathbf{W}^{(k)}\mathcal{F}\right\rangle = \Delta[\mathbf{W}^{(k)}\mathcal{F}]\,. \tag{2.13}$$

At this point it is also convenient to introduce the notation $\mathbf{F}_i^{(k)} = \left\langle v_i\mathbf{W}(\mathbf{v_i})^{(k)}\mathcal{F}\right\rangle$ for the flux corresponding to the conserved moment vector $\mathbf{U}^{(k)}$.

2.2.4 Grad Closure Hierarchy

According to Equation (2.13), it is strikingly clear that the evolution of $\mathbf{U}$ is related to $\mathcal{F}_i$. Due to the structure of Equation (2.13), $\mathcal{F}_i$ will always include moments of one order

higher than those in $\mathbf{U}$. These moments are not known and the system is not closed. In order to close this system of equations, one technique is to restrict the distribution function, $\mathcal{F}$, to have a prescribed form. This form should have the same number of free parameters, $\boldsymbol{\alpha} = [\alpha_1, \alpha_2, ..., \alpha_n]^T$, as the number of entries in the vector $\mathbf{U}$. The value of these parameters is chosen so that the moment relations are satisfied. Higher-order moments, that appears only on the flux, can then be integrated directly and become functions of known moment that are present in the solution vector.

In 1949, Grad [9] has proposed an assumed form for the distribution function to close the moment system. This proposition use a polynomial expansion around the equilibrium Maxwellian, $\mathcal{M}$, with the same density, momentum, and energy,

$$\mathcal{F}_{Grad} = \mathcal{M}\boldsymbol{\alpha}^T\boldsymbol{\phi}\,. \tag{2.14}$$

The Maxwellian distribution is the local equilibrium state of the gas. Inter-particle collisions move any gas to this state. The vector, $\boldsymbol{\phi}$, includes monomials of the particle velocity and $\boldsymbol{\alpha}$ contains the closure coefficients. As $\boldsymbol{\alpha}^T\boldsymbol{\phi}$ is a polynomial, it is possible for it to be negative. This means that theory would predict a negative number of particles at a location with a certain velocity. This, obviously, has no physical meaning. Also, the flux Jacobian of models of this type can develop complex eigenvalues. This results in a loss of hyperbolicity of the resulting PDEs, leading to ill-posed problems. The applicability of models in this family is obviously very limited.

2.2.5 Maximum-Entropy Moment Closures

Following Grad's proposition, a newer hierarchy of closures was proposed by assuming the distribution function is that which maximizes the entropy while remains consistent with moments present in the solution vector, **U**. Boltzmann proved that the entropy of a gas, that may be out of equilibrium, is given by $< -k\mathcal{F}\ln\mathcal{F} >$. Using the technique of Lagrange multipliers, it can be shown that the assumed form of $\mathcal{F}$ that maximizes their entropy while remaining consistent with the known moments in the solution vector has the form

$$\mathcal{F}_{\text{MaxEnt}} = e^{(\alpha^T \phi)} \,. \tag{2.15}$$

As the polynomial, $\boldsymbol{\alpha}^T\boldsymbol{\phi}$, is now in an exponential, the distribution function is positive valued, and for specific generating velocity weights in $\boldsymbol{\phi}$, the distribution stays finite. The maximum-entropy distribution is also statistically the most likely distribution that is consistent with the known moments. Also, after reviewed the useful mathematical properties of the maximum-entropy moment closures, it is clear that the resulting moment equations are globally hyperbolic. There are two commonly used low-order members of the maximum-entropy family. The first lowest-order member of this hierarchy is found by taking the generating weight to be $\mathbf{W} = [m, mv_i, mv_iv_i]^T$, which is known as the 5-moment closure. This closure results in the traditional compressible Euler equations of gas dynamics. The second lowest-order closure is derived from the maximum-entropy hierarchy by taking $\mathbf{W} = [m, mv_i, mv_iv_j]^T$. It is known as the 10-moment closures or the Gaussian closure [17]. The Gaussian closure gives a strictly hyperbolic treatment for viscous adiabatic gas flows. However, it does not have a treatment for heat flux. Unfortunately,

the maximum-entropy hierarchy has several issues related to the higher-order members of this maximum-entropy family. Firstly, for any moment systems that include third-order or higher-order moments, the vector of generating weights, $\boldsymbol{\phi}$, contains super-quadratic terms, moments of the distribution function cannot be expressed in closed form as the necessary integrals cannot be evaluated analytically. Secondly, Junk [16] has shown that there are physically realistic states for which closure coefficients that satisfy the moment relations do not exist. Both of these issues are explained in further detail in Chapter 4.

2.2.6 Application of Moment Closures to Multi-Phase Flow

The typical multi-phase situation of many particles is, in many ways, similar to that of a gas composed of a huge number of atoms or molecules. It is therefore expected that powerful techniques from the kinetic theory of gases could be applied. In this work, we define, $\mathbf{S}_i^{(k)}$, the source term due to the drag force between the fluid and particles. Equation(2.13) can then be rewritten compactly as

$$\frac{\partial \mathbf{U}^{(k)}}{\partial t} + \frac{\partial \mathbf{F}_i^{(k)}}{\partial x_i} + \mathbf{S}_i^{(k)} = \Delta[\mathbf{W}^{(k)}\mathcal{F}]\,, \tag{2.16}$$

where $\mathbf{S}_i^{(k)} = \left\langle \frac{\partial}{\partial v_i} a_i \mathbf{W}^{(k)}\mathcal{F} \right\rangle$ with the particle acceleration due to drag given by Equation (2.2). To investigate the most difficult physical cases, we are assuming that we have no collision operator. Equation (2.16) can then be given as

$$\frac{\partial \mathbf{U}^{(k)}}{\partial t} + \frac{\partial \mathbf{F}_i^{(k)}}{\partial x_i} = -\mathbf{S}_i^{(k)}\,. \tag{2.17}$$

Chapter 3

Review of Current Models For Multi-phase Flow Prediction

As Lagrangian treatments are often too expensive for practical use, Eulerian models are chosen. We start by reviewing the traditional single-velocity model. We show how this model could have been derived in the framework of kinetic theory and moment closures. We then show a range of other techniques and extensions, derived using this theory.

3.1 Single-Velocity Model

The traditional, single-velocity model assumes that; for a given position, x_i, and time, t; all particles have the same velocity. From the perspective of kinetic theory, this means the distribution function is a delta function,

$$\mathcal{F}_1 = \omega(x_i, t)\ \delta(v_i - \hat{v}_P(x_i, t))\,, \tag{3.1}$$

where $\omega(x_i, t)$ and $\hat{v}_P(x_i, t)$ are closure coefficients that must be chosen to ensure consistency with Equation (2.7), and δ is the Dirac delta function.

A graphical representation of this distribution function for one point in space and time

is shown in Figure 3.1. All the particles are concentrated on one velocity. By substituting Equation (3.1) into Equation (2.11), and choosing as velocity weights $W_1 = m$, and $W_2 = mv_i$, the distribution function has moments

$$\begin{aligned} \rho &= \langle m\mathcal{F} \rangle \ , \\ \rho u_i &= \langle m v_i \mathcal{F} \rangle \ . \end{aligned} \tag{3.2}$$

The following conservation model for particle flow can be found:

$$\frac{\partial \mathbf{U}}{\partial t} + \frac{\partial \mathbf{F}_k}{\partial x_k} = \mathbf{S} \, , \tag{3.3}$$

with

$$\mathbf{U} = \begin{bmatrix} \rho \\ \\ \rho u_i \end{bmatrix} \quad , \quad \mathbf{F}_k = \begin{bmatrix} \rho u_k \\ \\ \rho u_i u_k \end{bmatrix} \quad \text{and} \quad \mathbf{S} = \begin{bmatrix} 0 \\ \\ (\rho/\tau)(u_{gi} - u_i) \end{bmatrix} . \tag{3.4}$$

Where $\mathbf{U}$ and $\mathbf{F}_k$ are the solution vector and flux dyad respectively and $\mathbf{S}$ is a vector denoting the source term due to the drag force between the fluid and particles. Here, u_{gi} is the background fluid velocity and the value of τ comes from the assumption of Stokes flow, and has the value

$$\tau = \frac{\rho_p d_p^2}{\mu_g 18} \, . \tag{3.5}$$

This system comprises one scalar and one vector equation for the conservation of mass and momentum of the particle phase. The single-velocity model forces all particles to have the same velocity at a point in space, but allows it to be different than the background fluid velocity. However, restricting all particles at one location to have the same velocity obviously renders this model inappropriate when the situation comprises multiple particle velocities at any point in the flow. Though this is the most commonly used model, it suffers from several major disadvantages. For example, if there are two or more groups

of intersecting particle flows, particle crossing is impossible. Also, only a limited number of boundary conditions can be applied. For example, reflective boundary conditions are impossible, as was proved by both Slater [29] and Sachdev [26].

Eigenstructure for Two-Dimensional Flows

As with all models considered in this work, the resultant moment system takes the form of first-order hyperbolic balance laws. The solution of such laws is in terms of waves that are characterized by the eigenstructure of the flux Jacobians. For two space dimensions, this model can be expressed in Cartesian coordinates as

$$\frac{\partial \mathbf{U}}{\partial t} + \frac{\partial \mathbf{F}_x}{\partial x} + \frac{\partial \mathbf{F}_y}{\partial y} = \mathbf{S}\,, \tag{3.6}$$

where again $\mathbf{U}$ is the vector of conserved variables which can be expressed as

$$\mathbf{U} = \begin{bmatrix} \rho \\ \rho u_x \\ \rho u_y \end{bmatrix}, \tag{3.7}$$

The source vector, $\mathbf{S}$, of Equation (3.6) has the form:

$$\mathbf{S} = \begin{bmatrix} 0 \\ \frac{\rho(u_{gx}-u_x)}{\tau} \\ \frac{\rho(u_{gy}-u_y)}{\tau} \end{bmatrix}, \tag{3.8}$$

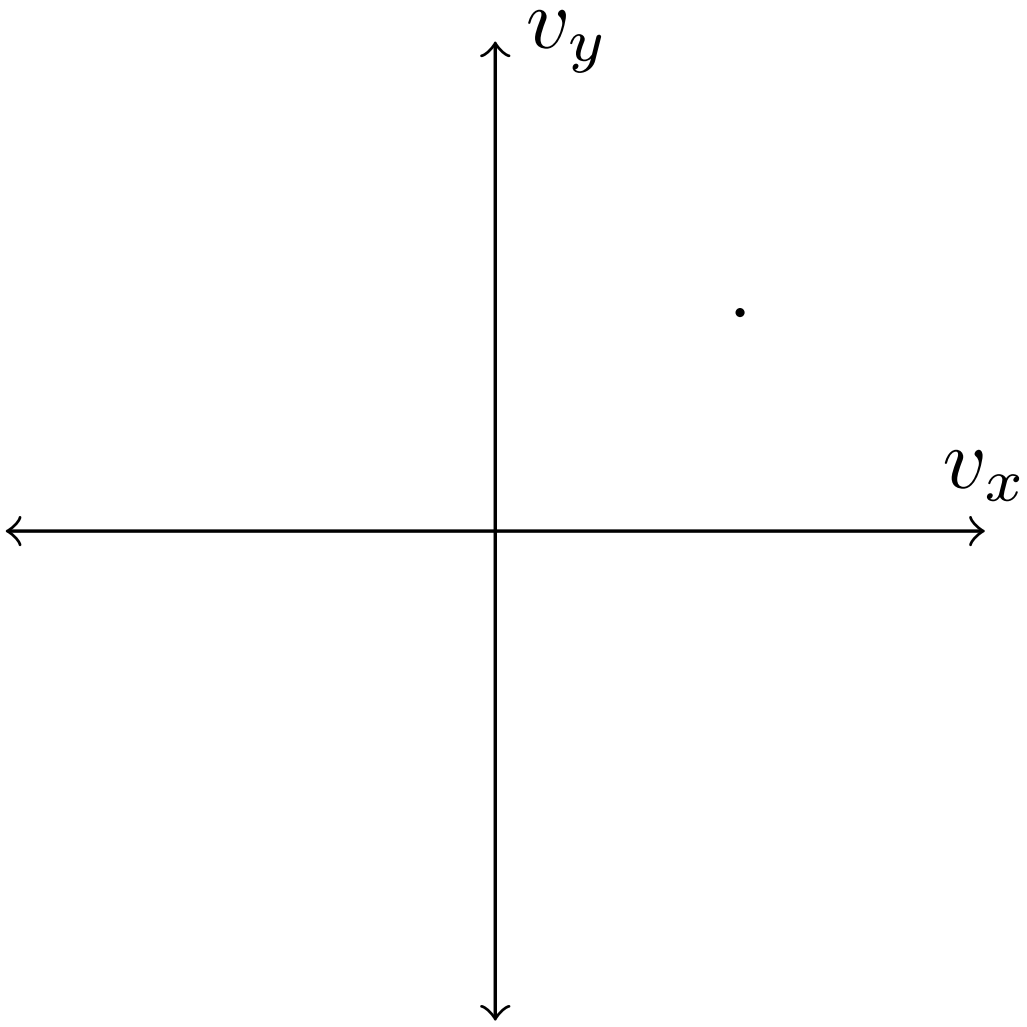

Figure 3.1: *Example of a distribution function at one point in space corresponding to the single-velocity model*

while $\mathbf{F}_x$ and $\mathbf{F}_y$ are x- and y-direction fluxes given by

$$\mathbf{F}_x = \begin{bmatrix} \rho u_x \\ \rho u_x^2 \\ \rho u_x u_y \end{bmatrix}, \quad \mathbf{F}_y = \begin{bmatrix} \rho u_y \\ \rho u_x u_y \\ \rho u_y^2 \end{bmatrix}. \tag{3.9}$$

By making use of the flux-Jacobian matrices $\mathbf{A} = \frac{\partial \mathbf{F}_x}{\partial U}$ and $\mathbf{B} = \frac{\partial \mathbf{F}_y}{\partial U}$, Equation (3.6) can be rewritten as

$$\frac{\partial \mathbf{U}}{\partial t} + \mathbf{A}\frac{\partial \mathbf{U}}{\partial x} + \mathbf{B}\frac{\partial \mathbf{U}}{\partial y} = \mathbf{S}, \tag{3.10}$$

As this model is invariant under rotation, an investigation of the x-direction Jacobian suffices to describe the system. This Jacobian is given as

$$\mathbf{A} = \begin{bmatrix} 0 & 1 & 0 \\ -u_x^2 & 2u_x & 0 \\ -u_x u_y & u_y & u_x \end{bmatrix}. \tag{3.11}$$

The eigenvalues for $\mathbf{A}$ are:

$$\lambda_{1-3} = (\ u_x,\ u_x,\ u_x\ ).$$

The corresponding eigenvectors for the conserved variables are:

$$r_1 = \begin{bmatrix} 0 \\ 0 \\ 1 \end{bmatrix}, \ r_2 = \begin{bmatrix} \frac{1}{u_x} \\ 1 \\ 0 \end{bmatrix}, \ r_3 = \begin{bmatrix} 0 \\ 0 \\ 0 \end{bmatrix},$$

The speed of information propagation in hyperbolic systems is given by the eigenvalues of $\mathbf{A}$. It can be seen that, for this single-velocity system, all information moves with the particle velocity, u_i. The right eigenvectors are also listed as they are often important for

the numerical solution of such systems.

3.1.1 Multi-Velocity Models

Once this classical model is seen through the lens of kinetic theory, it is natural to consider extending the law by allowing multiple discrete velocities at any point in space [23, 5]. This is done by assuming $\mathcal{F}$ to be composed of multiple delta functions,

$$\mathcal{F}_M = \sum_{k=0}^{N} \omega^{(k)}(x_i, t)\ \delta(v_i - \hat{v}_i^{(k)}(x_i, t)) \qquad N \geq 2. \tag{3.12}$$

Figure (3.2), shows an illustration of how such a distribution function may appear. In this case, it is assumed that, at any point in space and time, particles can have any of six velocities. These six velocities need not be the same for every point in space.

It is often not possible to analytically determine the weights and locations of the delta functions in the assumed distribution. Rather, a relatively expensive numerical inversion algorithm must be used to determine the moment relation each time a flux evaluation is needed. In order to render this inversion simpler, it is often assumed that the delta functions must exist on a small number of lines in $v_x - v_y$ space. The resulting models remain numerically expensive and lose Galilean invariance. Such methods are not considered further in this work.

3.2 Euler Model

Once the idea of multiple delta functions is abandoned, the next logical thought is to allow the single delta function to expand to a continuous distribution. For this work, we do

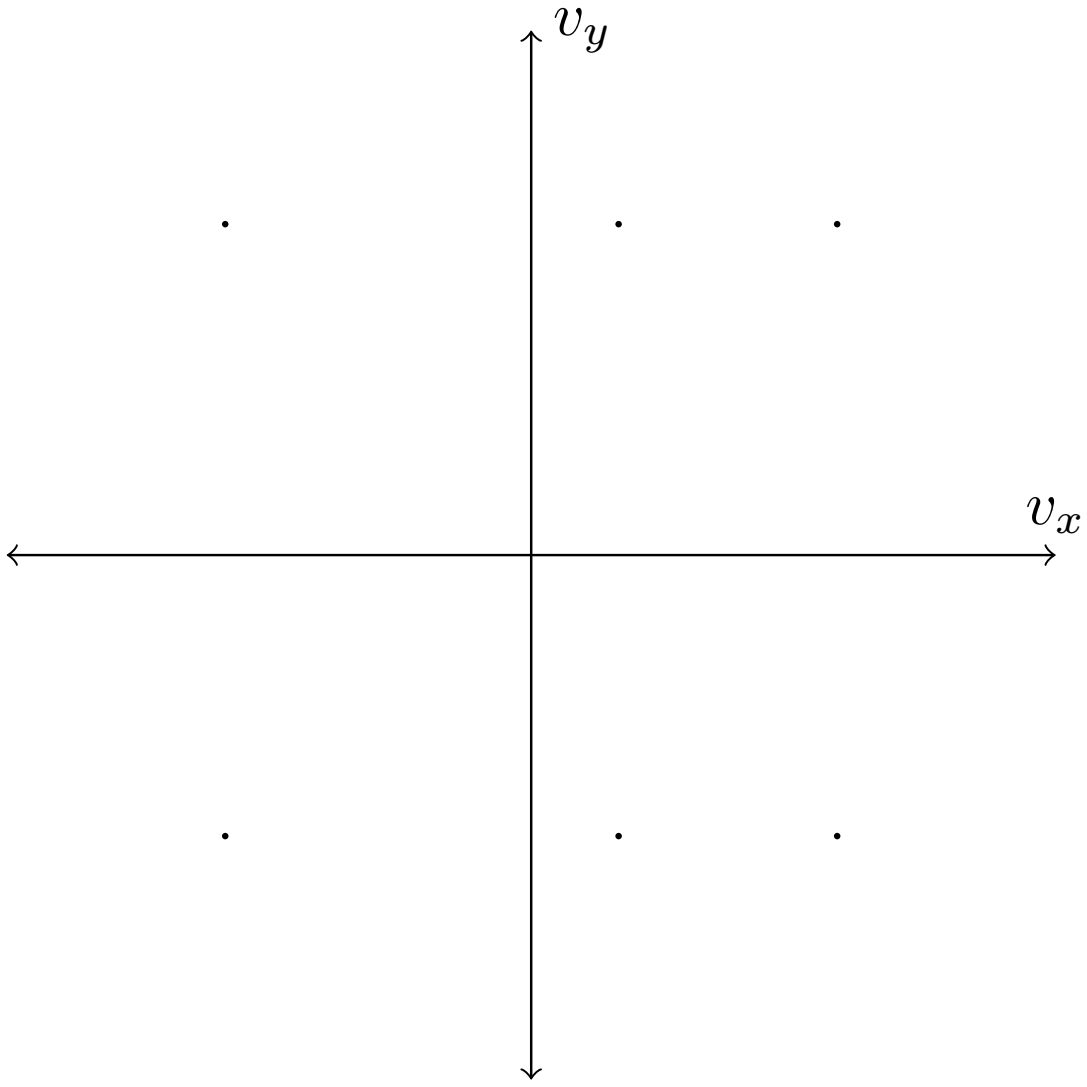

Figure 3.2: *Illustration of a distribution function corresponding to the multi-velocity model*

this by following the maximum-entropy hierarchy, introduced in Section 2.2.5. As stated earlier, the lowest-order member of this theory is a five-moment system that results in the compressible Euler equations. The assumed distribution function is

$$\mathcal{M} = \mathcal{F}_E = \frac{\rho}{m}\sqrt{\frac{\rho}{2\pi p}}\exp\left(-\frac{\rho}{2p}c_i c_i\right) . \tag{3.13}$$

An illustration of this distribution function is shown in Figure 3.3. It can be seen that, at a location, x_i, there is a single particle velocity that most likely, but now there is a significant standard deviation. This distribution function has moments:

$$\begin{aligned}
\rho &= \langle m\mathcal{F}\rangle \ , \\
\rho u_i &= \langle m v_i \mathcal{F}\rangle \ , \\
\frac{\rho u_i u_i}{2} + \frac{3p}{2} &= \left\langle \frac{m v_i v_i \mathcal{F}}{2}\right\rangle , \\
\rho u_i u_j + \delta_{ij} p &= \langle m v_i v_j \mathcal{F}\rangle \ , \\
\rho u_j(\frac{5p}{2} + \frac{\rho(u_i u_i)}{2}) &= \left\langle \frac{m v_j v_i v_i \mathcal{F}}{2}\right\rangle .
\end{aligned} \tag{3.14}$$

If this equilibrium distribution function is substituted into Maxwell's equation of change, the result is a five-moment system that can be written as

$$\frac{\partial \rho}{\partial t} + \frac{\partial}{\partial x_i}(\rho u_i) = 0 , \tag{3.15}$$

$$\frac{\partial}{\partial t}(\rho u_i) + \frac{\partial}{\partial x_j}(\rho u_i u_j + \delta_{ij} p) = \frac{\rho(u_{gi} - u_i)}{\tau} , \tag{3.16}$$

$$\frac{\partial}{\partial t}(\frac{3p}{2} + \frac{\rho(u_i u_i)}{2}) + \frac{\partial}{\partial x_j}(\rho u_j(\frac{5p}{2} + \frac{\rho(u_i u_i)}{2})) = \frac{\rho u_i(u_{gi} - u_i) + \rho u_j(u_{gj} - u_j) - 3p}{\tau} . \tag{3.17}$$

This is identical to the traditional compressible Euler-equations for a monatomic gas, except there is now a source term that accounts for particle drag. The balance law can be

expressed as

$$\frac{\partial \mathbf{U}}{\partial t} + \frac{\partial \mathbf{F}_k}{\partial x_k} = \mathbf{S} \tag{3.18}$$

Where

$$\mathbf{U} = \begin{bmatrix} \rho \\ \rho u_i \\ \frac{3p}{2} + \frac{\rho(u_i u_i)}{2} \end{bmatrix} \quad ; \quad \mathbf{F}_k = \begin{bmatrix} \rho u_i \\ \rho u_i u_j + \delta_{ij} p \\ \rho u_j (\frac{3p}{2} + \frac{\rho(u_i u_i)}{2}) \end{bmatrix} \quad \text{and} \quad \mathbf{S} = \begin{bmatrix} 0 \\ \frac{\rho(u_{gi} - u_i)}{\tau} \\ \frac{\rho u_i(u_{gi} - u_i) + \rho u_j(u_{gj} - u_j) - 3p)}{\tau} \end{bmatrix}. \tag{3.19}$$

Eigenstructure for Two-Dimensional Flows:

Again, in order to evaluate the wave behaviour of the Euler system, it is necessary to study the eigenstructure of this model. We need to calculate the eigenvalues and eigenvectors for the flux Jacobian. The system, expressed in two-dimensional Cartesian coordinates, is

$$\frac{\partial \mathbf{U}}{\partial t} + \frac{\partial \mathbf{F}_x}{\partial x} + \frac{\partial \mathbf{F}_y}{\partial y} = \mathbf{S}\,. \tag{3.20}$$

Where again $\mathbf{U}$ is the vector of conserved variables which can be expressed as:

$$\mathbf{U} = \begin{bmatrix} \rho \\ \rho u_x \\ \rho u_y \\ \frac{3p}{2} + \frac{\rho(u_x^2 + u_y^2)}{2} \end{bmatrix}, \tag{3.21}$$

The source vector $\mathbf{S}$ of equation. (3.20) has the form:

$$\mathbf{S} = \begin{bmatrix} 0 \\ \frac{\rho(V_x - u_x)}{\tau} \\ \frac{\rho(V_y - u_y)}{\tau} \\ \frac{\rho u_x(V_x - u_x) + \rho u_y(V_y - u_y) - 3p}{\tau} \end{bmatrix}, \tag{3.22}$$

While $\mathbf{F}_x$ is the x-direction flux, given by

$$\mathbf{F}_x = \begin{bmatrix} \rho u_x \\ \rho u_x^2 + p \\ \rho u_x u_y \\ u_x(\frac{5p}{2} + \frac{\rho(u_x^2 + u_y^2)}{2}) \end{bmatrix}. \tag{3.23}$$

By making use of the flux-Jacobian matrix: $\mathbf{A} = \frac{\partial \mathbf{F}_x}{\partial \mathbf{U}}$ and $\mathbf{B} = \frac{\partial \mathbf{F}_y}{\partial \mathbf{U}}$, Equation (3.20) can also be rewritten as

$$\frac{\partial \mathbf{U}}{\partial t} + \mathbf{A}\frac{\partial \mathbf{U}}{\partial x} + \mathbf{B}\frac{\partial \mathbf{U}}{\partial y} = \mathbf{S}. \tag{3.24}$$

The Jacobian $\mathbf{A} = \frac{\partial \mathbf{F}_x}{\partial \mathbf{U}}$ can be written as

$$\mathbf{A} = \begin{bmatrix} 0 & 1 & 0 & 0 \\ \frac{u_x^2(\frac{5}{3}-3)+(u_y^2)(\frac{5}{3}-1)}{2} & u_x(3-\frac{5}{3}) & u_y(1-\frac{5}{3}) & \frac{5}{3}-1 \\ -u_x u_y & u_y & u_x & 0 \\ \frac{u_x(\rho(u_x^2+u_y^2)(\frac{5}{3}^2-3\frac{5}{3}+2)-2\frac{5}{3}p}{2\rho(\frac{5}{3}-1)} & \frac{p}{\rho(\frac{5}{3}-1)} - \frac{(u_x^2+u_y^2)}{2} + \frac{p}{\rho} + u_x^2(\frac{5}{3}-1) & u_x u_y(1-\frac{5}{3}) & u_x\frac{5}{3} \end{bmatrix} \tag{3.25}$$

The eigenvalues of the matrix $\mathbf{A}$ in equation(3.25) are u, u, $u+a$, and $u-a$. Here, a

is the speed of sound, with $a = \sqrt{\frac{5p}{3\rho}}$ for a monatomic gas. The right eigenvectors of the matrix are

$$V_1 = \begin{bmatrix} 1 \\ u-a \\ v \\ H-ua \end{bmatrix}, V_2 = \begin{bmatrix} 1 \\ u \\ v \\ \frac{(u^2+v^2)}{2} \end{bmatrix}, V_3 = \begin{bmatrix} 0 \\ 0 \\ 1 \\ v \end{bmatrix}, V_4 = \begin{bmatrix} 1 \\ u+a \\ v \\ H+ua \end{bmatrix},$$

with specific enthalpy

$$\mathbf{H} = \frac{(E+p)}{\rho}, \tag{3.26}$$

where $E = \frac{3p}{2} + \frac{\rho(u_x^2+u_y^2)}{2}$ is the energy density.

3.3 Gaussian Model

The next lowest-order member of the maximum-entropy hierarchy is the Gaussian model. In 1867, Maxwell [19] seems to have been the first researcher who inferred the Gaussian distribution. After almost one hundred years, Holway [12, 13, 14, 15] and Schlüter [11, 24] both rediscover it. For the Gaussian closure, the velocity distribution function is assumed to have the form

$$\mathcal{F}_{\mathrm{G}} = \frac{\rho}{m(2\pi)^{3/2}(\det \Theta_{ij})^{1/2}} e^{\left(-\frac{1}{2}\Theta_{ij}^{-1} c_i c_j\right)}. \tag{3.27}$$

Where $\Theta_{ij} = P_{ij}/\rho$ is an anisotropic "temperature" tensor. An example of this distribution function is illustrated in Figure 3.4. It can be seen that it is similar to the Euler distribution, except lines of constant probability are now stretched into ellipses. In other words, the standard deviation of particle velocities is now different in different directions. The moment equations corresponding to the Gaussian closure can be obtained by using

the weights $\boldsymbol{W}^{(10)} = \{1, v_i, v_i v_j\}$. When the resulting distribution function, is used in Maxwell's equation of change, Equation (3.6), the result is a set of ten partial-differential equations describing the transport of the macroscopic quantities ρ, u_i, and P_{ij}, which may be expressed as

$$\frac{\partial \rho}{\partial t} + \frac{\partial}{\partial x_k}(\rho u_k) = 0\,, \tag{3.28}$$

$$\frac{\partial}{\partial t}(\rho u_i) + \frac{\partial}{\partial x_k}(\rho u_i u_k + P_{ik}) = \mathbf{S}_2\,, \tag{3.29}$$

$$\frac{\partial}{\partial t}(P_{ij} + \rho u_i u_j) + \frac{\partial}{\partial x_k}(\rho u_i u_j u_k + u_i P_{jk} + u_j P_{ik} + u_k P_{ij}) = \mathbf{S}_3\,. \tag{3.30}$$

Here, Equation (3.28) represents the continuity equation, Equation (3.29) represents the momentum equation and Equation (3.30) is a tensor equation for a symmetric energy tensor.

Eigenstructure for Two-Dimensional Flow:

Against the behaviours of the system is described by the eigenstructure of the flux Jacobians. The balance laws are again expressed in two-dimensional Cartesian coordinates as

$$\frac{\partial \mathbf{U}}{\partial t} + \frac{\partial \mathbf{F}_x}{\partial x} + \frac{\partial \mathbf{F}_y}{\partial y} = \mathbf{S}\,, \tag{3.31}$$

where again $\mathbf{U}$ is the vector of conserved variables which can be expressed as

$$\mathbf{U} = \begin{bmatrix} \rho \\ \rho u_x \\ \rho u_y \\ \rho u_x^2 + P_{xx} \\ \rho u_x u_y + P_{xy} \\ \rho u_y^2 + P_{yy} \\ P_{zz} \end{bmatrix}, \tag{3.32}$$

while $\mathbf{F}_x$ and $\mathbf{F}_y$ are x- and y-direction fluxes given by

$$\mathbf{F}_x = \begin{bmatrix} \rho u_x \\ \rho u_x^2 + P_{xx} \\ \rho u_x u_y + P_{xy} \\ \rho u_x^3 + 3u_x P_{xx} \\ \rho u_x^2 u_y + 2u_x P_{xy} + u_y P_{xx} \\ \rho u_x u_y^2 + u_x P_{yy} + 2u_y P_{xy} \\ u_x P_{zz} \end{bmatrix}, \quad \mathbf{F}_y = \begin{bmatrix} \rho u_y \\ \rho u_x u_y + P_{xy} \\ \rho u_y^2 + P_{yy} \\ \rho u_x^2 u_y + 2u_x P_{xy} + u_y P_{xx} \\ \rho u_x u_y^2 + u_x P_{yy} + 2u_y P_{xy} \\ \rho u_y^3 + 3u_y P_{yy} \\ u_y P_{zz} \end{bmatrix}. \tag{3.33}$$

The source vector, $\mathbf{S}$,of Equation (3.31) has the form

$$\mathbf{S} = \begin{bmatrix} 0 \\ \frac{\rho}{\tau}(u_{gx} - u_x) \\ \frac{\rho}{\tau}(u_{gy} - u_y) \\ \frac{2}{\tau}(\rho u_x(u_{gx} - u_x) - P_{xx}) \\ \frac{1}{\tau}(\rho u_y(u_{gx} - u_x) + \rho u_x(u_{gy} - u_y) - 2P_{xy}) \\ \frac{2}{\tau}(\rho u_y(u_{gy} - u_y) - P_{yy}) \\ -\frac{2}{\tau}P_{zz} \end{bmatrix},$$

By again making use of the Jacobians $\mathbf{A} = \frac{\partial \mathbf{F}_x}{\partial \mathbf{U}}$ and $\mathbf{B} = \frac{\partial \mathbf{F}_y}{\partial \mathbf{U}}$, Equation(3.31) can also be rewritten as

$$\frac{\partial \mathbf{U}}{\partial t} + \mathbf{A}\frac{\partial \mathbf{U}}{\partial x} + \mathbf{B}\frac{\partial \mathbf{U}}{\partial y} = \mathbf{S}\,. \tag{3.34}$$

The Jacobian $\mathbf{A} = \frac{\partial \mathbf{F}_x}{\partial \mathbf{U}}$ can be written as:

$$\mathbf{A} = \begin{bmatrix} 0 & 1 & 0 & 0 & 0 & 0 & 0 \\ 0 & 0 & 0 & 1 & 0 & 0 & 0 \\ 0 & 0 & 0 & 0 & 1 & 0 & 0 \\ -3u_x c_{xx}^2 + u_x^3 & 3(c_{xx}^2 - u_x^2) & 0 & 3u_x & 0 & 0 & 0 \\ (u_x^2 u_y) - \frac{P_y u_x + 2u_y P_{xy}}{\rho} & \frac{-2P_{xy}}{\rho} - 2u_y u_x & c_{xx}^2 - u_x^2 & u_y & 2u_x & 0 & 0 \\ (u_x u_y^2) - \frac{u_x P_{yy} - 2u_y P_{xy}}{\rho} & \frac{P_{yy}}{\rho} - u_y^2 & \frac{2P_{xy}}{\rho} & 0 & 2u_y & u_x & 0 \\ \frac{-P_{zz}u_x}{\rho} & \frac{P_{zz}}{\rho} & 0 & 0 & 0 & 0 & u_x \end{bmatrix}. \tag{3.35}$$

The eigenvalues and right and left eigenvectors must be determined for $\mathbf{A}$. Using $\rho c_{xx}^2 =$

P_{xx} , the eight eigenvalues of $\mathbf{A}$ are

$$\lambda_{1-7} = \left(u_x - \sqrt{3}c_{xx},\ u_x - c_{xx},\ u_x,\ u_x,\ u_x,\ u_x + c_{xx},\ u_x + \sqrt{3}c_{xx} \right) .$$

These represent the wave speeds of the fundamental solution modes for the model. The corresponding right eigenvectors are

$$r_{c1} = \begin{bmatrix} 1 \\ u_x - \sqrt{3}c_{xx} \\ u_y - \frac{\sqrt{3}P_{xy}}{c_{xx}\rho} \\ 3c_{xx}^2 - 2\sqrt{3}u_x c_{xx} + {u_x}^2 \\ \frac{u_x \rho u_y c_{xx} - u_x\sqrt{3}P_{xy} - \sqrt{3}c_{xx}^2 \rho u_y + 3c_{xx}P_{xy}}{c_{xx}\rho} \\ \frac{\rho^2 u_y^2 c_{xx}^2 - 2\sqrt{3}P_{xy}c_{xx}\rho u_y + \rho c_{xx}^2 P_{yy} + 2P_{xy}^2}{\rho^2 c_{xx}^2} \\ \frac{P_{zz}}{\rho} \end{bmatrix} , r_{c2} = \begin{bmatrix} 0 \\ 0 \\ 1 \\ 0 \\ u_x - c_{xx} \\ 2\left(u_y - \frac{P_{xy}}{c_{xx}\rho}\right) \\ 0 \end{bmatrix} ,$$

$$r_{c3} = \begin{bmatrix} 1 \\ u_x \\ u_y \\ u_x^2 \\ u_x u_y \\ u_y^2 \\ 0 \end{bmatrix} , r_{c4} = \begin{bmatrix} 0 \\ 0 \\ 0 \\ 0 \\ 0 \\ 1 \\ 0 \end{bmatrix} , r_{c5} = \begin{bmatrix} 0 \\ 0 \\ 0 \\ 0 \\ 0 \\ 0 \\ 1 \end{bmatrix} ,$$

$$r_{c6} = \begin{bmatrix} 0 \\ 0 \\ 1 \\ 0 \\ u_x + c_{xx} \\ 2\left(u_y + \frac{P_{xy}}{c_{xx}\rho}\right) \\ 0 \\ 0 \end{bmatrix}, \; r_{c7} = \begin{bmatrix} 1 \\ u_x + \sqrt{3}c_{xx} \\ u_y + \frac{\sqrt{3}P_{xy}}{c_{xx}\rho} \\ 3c_{xx}^2 + 2\sqrt{3}u_x c_{xx} + {u_x}^2 \\ \frac{u_x \rho u_y c_{xx} + u_x \sqrt{3} P_{xy} + \sqrt{3} c_{xx}^2 \rho u_y + 3 c_{xx} P_{xy}}{c_{xx}\rho} \\ \frac{\rho^2 u_y^2 c_{xx}^2 + 2\sqrt{3} P_{xy} c_{xx} \rho u_y + \rho c_{xx}^2 P_{yy} + 2 P_{xy}^2}{\rho^2 c_{xx}^2} \\ \frac{P_{zz}}{\rho} \end{bmatrix}.$$

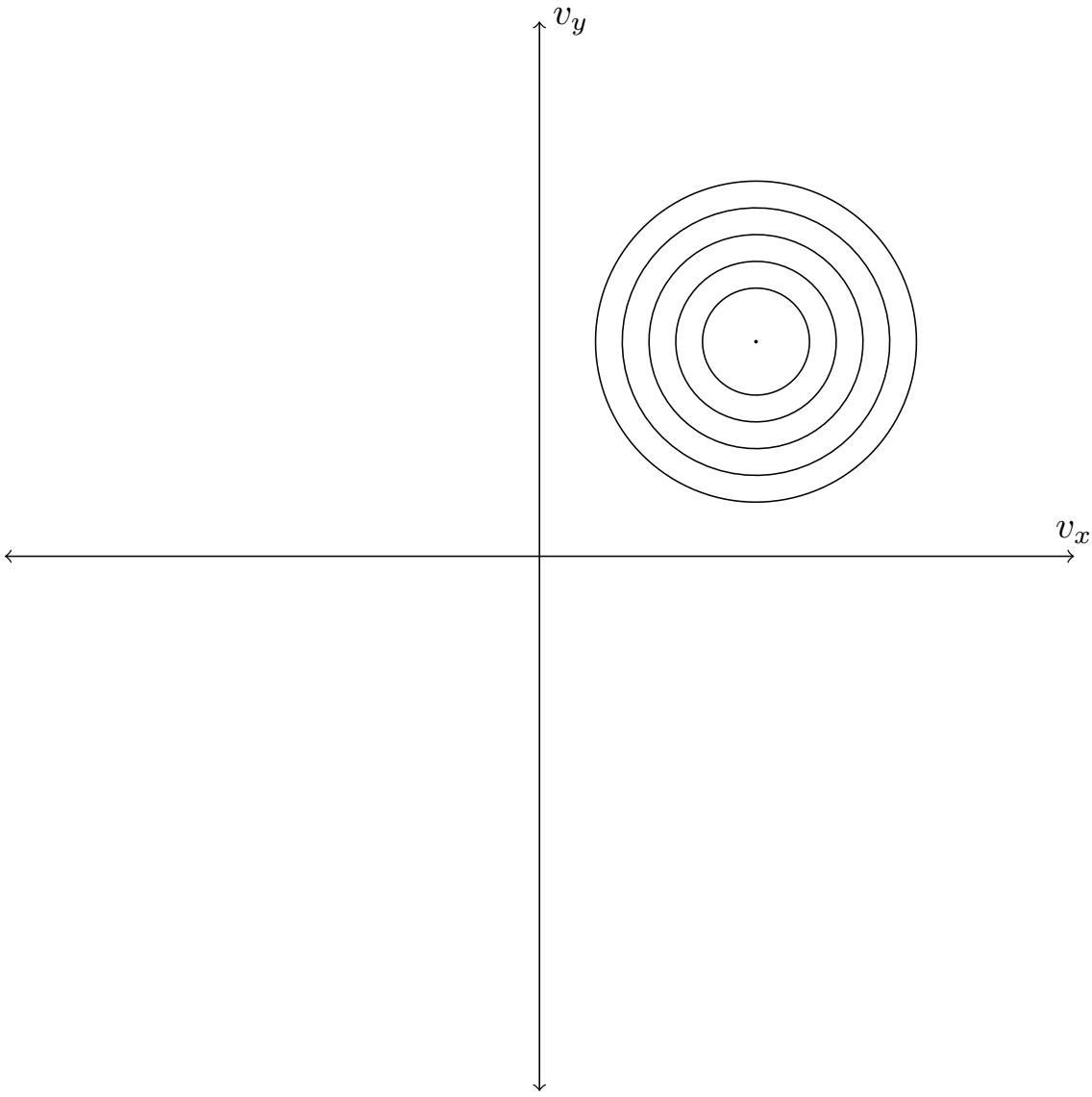

Figure 3.3: *Illustration of a typical assumed distribution function for the Euler closure*

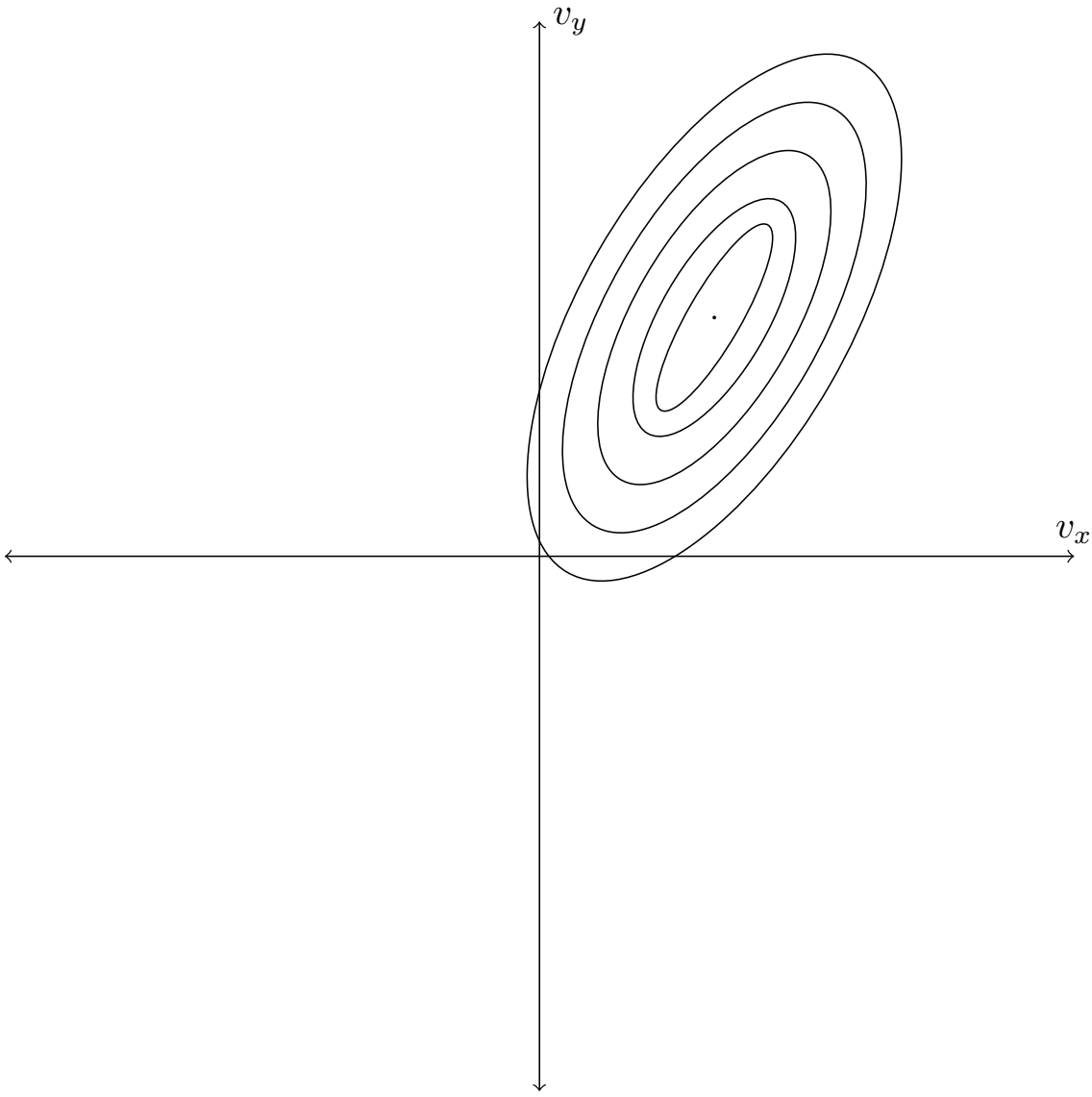

Figure 3.4: *Illustration of a typical assumed distribution function for Gaussian closure*

Chapter 4

Fourteen-Moment Closure Model

4.1 Closed-Form Approximation to Maximum-Entropy Closures

The success of the 5 and the 10-moment maximum-entropy closures to produce ever-more flexible models gives confidence that higher-order models should be easily produced. Unfortunately, for the next member of the theory, a 14-moment closure, the two issues mentioned earlier become problematic. The vector of generating weights for this closure is $\phi = [m, mv_i, mv_iv_j, mv_iv_jv_j, mv_iv_iv_jv_j]$. This produces a quadratic polynomial, $\boldsymbol{\alpha}^T\boldsymbol{\phi}$, in the distribution function. Figure 4.1 shows an illustration of a general form that this distribution can take. It can be seen that bi-modal distributions are now possible.

Evaluation the moments of this distribution would require integration functions of the form

$$\int \mathcal{F}(x_i, v_i, t) = \int e^{(\alpha_0+\alpha_1 v+\alpha_2 v^2+\alpha_3 v^3+\alpha_4 v^4)} \mathrm{d}v \,. \tag{4.1}$$

A solution of such an integral is unknown. The result of this is that, given a set of known moments, the corresponding closure coefficients, $\boldsymbol{\alpha}$, can only be found through an expensive, poorly conditioned iterative process. Also, Junk has shown that these exist

physically possible states for which no distribution with maximum entropy exists [20]. In order to circumvent these issues, McDonald and Torrilhon have recently proposed a new interpolative procedure that approximates the true closure [20]. The main points of this new procedure are summarized here.

The moments that fill the solution vector for this model are

$$\rho = \langle m\mathcal{F} \rangle , u_i = \frac{\langle mv_i\mathcal{F} \rangle}{\rho}, P_{ij} = \langle mc_ic_j\mathcal{F} \rangle , Q_{ijj} = \left\langle mc_ic^2\mathcal{F} \right\rangle , R_{iijj} = \left\langle mc^4\mathcal{F} \right\rangle \ ,$$

where, Q_{ijj} is the heat flux vector and R_{iijj} is a forth-order moment. The resulting system of moment equations is:

$$\begin{aligned}
&\frac{\partial \rho}{\partial t} + \frac{\partial}{\partial x_i} (\rho u_i) = 0 \\
&\frac{\partial}{\partial t} (\rho u_i) + \frac{\partial}{\partial x_j} (\rho u_j u_i + P_{ij}) = \mathbf{S}_2 \\
&\frac{\partial}{\partial t} (\rho u_i u_j + P_{ij}) + \frac{\partial}{\partial x_k} (\rho u_j u_i u_k + P_{jk} u_i + u_j P_{ik} + u_k P_{ij} + Q_{ijk}) = \mathbf{S}_3 \\
&\frac{\partial}{\partial t} (\rho u_i u_j u_j + u_i P_{jj} + 2u_j P_{ij} + Q_{ijj}) + \frac{\partial}{\partial x_k} (\rho u_i u_k u_j u_j + P_{jj} u_i u_k + \\
&2u_i u_j P_{jk} + 2u_j u_k P_{ij} + u_j u_j P_{ik} + u_i Q_{kjj} + u_k Q_{ijj} + 2u_j Q_{ijk} + R_{ikjj}) = \mathbf{S}_4 \\
&\frac{\partial}{\partial t} (\rho u_i u_i u_j u_j + 2u_i u_i P_{jj} + 4u_i u_j P_{ij} + 4u_i Q_{ijj} + R_{iijj}) + \\
&\frac{\partial}{\partial x_k} (\rho u_k u_i u_i u_j u_j + 2u_k u_i u_i P_{jj} + 4u_i u_i u_j P_{jk} + 4u_i u_j u_k P_{ij} + 2u_i u_i Q_{kjj} + \\
&4u_i u_k Q_{ijj} + 4u_i u_j Q_{ijk} + 4u_i R_{ikjj} + u_k R_{iijj} + S_{kiijj}) = \mathbf{S}_5 \, .
\end{aligned}$$

To close this system of PDEs, we must find expression for moments which appear only in the flux dyad. These are

$$S_{ijjkk} = \left\langle mc_ic^4\mathcal{F} \right\rangle , \ R_{ijkk} = \left\langle mc_ic_jc^2\mathcal{F} \right\rangle , \text{ and } Q_{ijk} = \langle mc_ic_jc_k\mathcal{F} \rangle ,$$

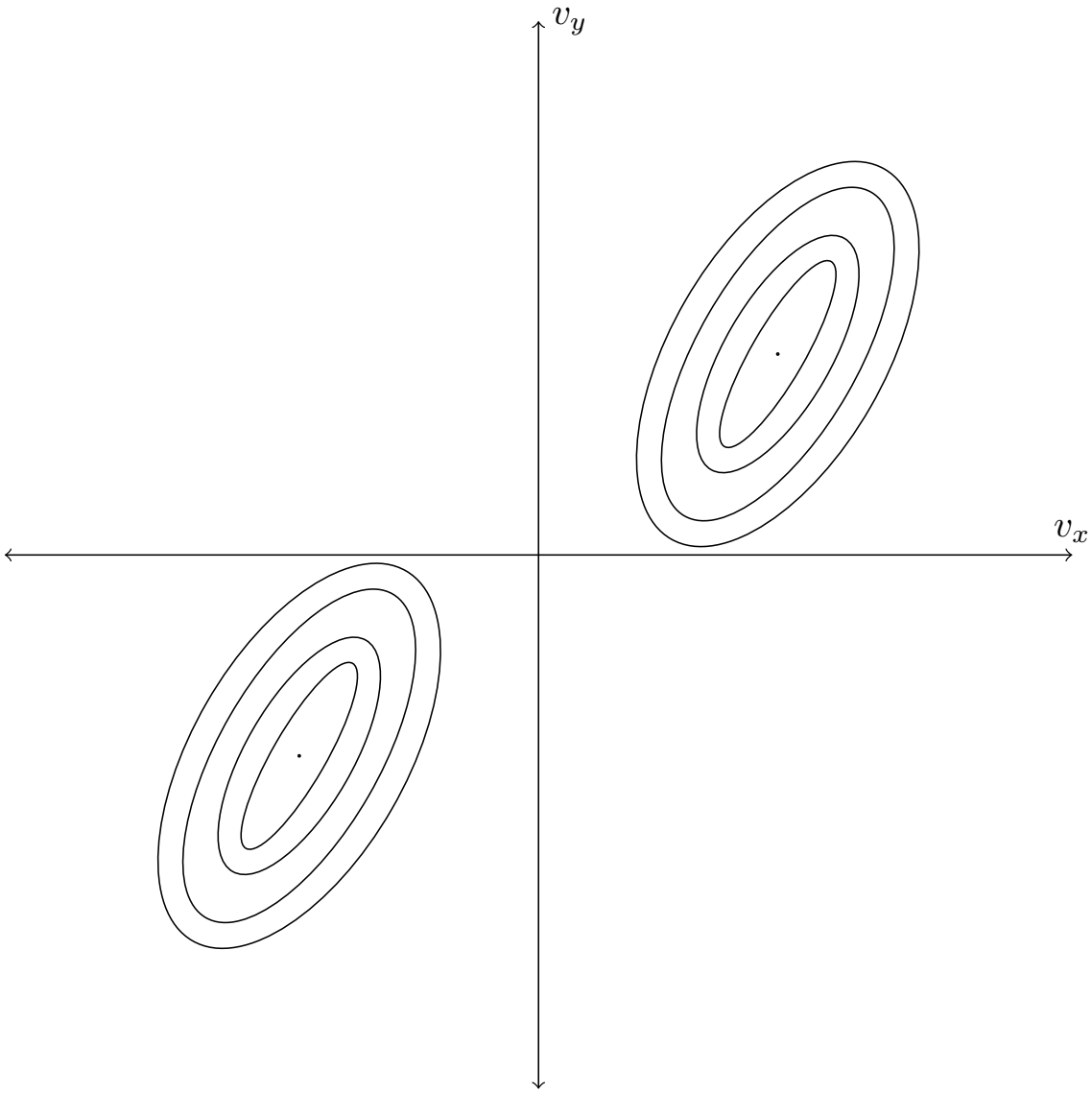

Figure 4.1: *Illustrative representation of a Fourteen-moment maximum-entropy distribution function*

The closing procedure proposed by McDonald and Torrilhon is based on an interpolation procedure between limits of realizability. There are two limits of realizability for this closure. First, there are limits to physical realizable. Just as density and pressure can never be negative in reality, it can be shown that the forth moment, R_{iijjj} cannot be less than $Q_{ijj}P^{-1}_{ik}Q_{kll} + \frac{P_{ii}P_{jj}}{\rho}$, a quadratic function of Q_{ijj}. For the maximum-entropy theory, there is another limit. It represents the region of physically possible states for which the entropy maximization problem has no solution. This limit is all states for which $Q_{xii} = 0$ and $R_{iijj} > \frac{2P_{ji}P_{ij}+P_{ii}P_{jj}}{\rho}$. The states where

$$R_{iijj} = \frac{2P_{ji}P_{ij} + P_{ii}P_{jj}}{\rho}$$

correspond to the 10-moment Gaussian closure. So, if there is no heat flux, the fourth moment cannot be higher than that predicted by the 10-moment model. A simplified illustration of these two limits is shown in Figure 4.2. On both of these realizable limits, it is possible to gain knowledge about the missing terms in the flux dyad. By defining an interpolation coefficient, σ, McDonald and Torrilhon used this boundary knowledge to propose approximation to the missing terms. The coefficient σ is defined as

$$\sigma = \frac{[2P_{ij}P_{ji} + P_{ii}P_{jj} - \rho R_{iijj}] + \sqrt{([2P_{ij}P_{ji} + P_{ii}P_{jj} - \rho R_{iijj}]^2 + 8\rho P_{mn}P_{nm}Q_{kii}(P^{-1})_{kl}Q_{ljj})}}{4P_{ij}P_{ji}} \tag{4.2}$$

This has value zero on the Junk region where

$$Q_{xii} = 0 \quad \text{and} \quad R_{iijj} > \frac{2P_{ji}P_{ij} + P_{ii}P_{jj}}{\rho}$$

and value one on the limit of physical realizability. The postulated closing moment relations

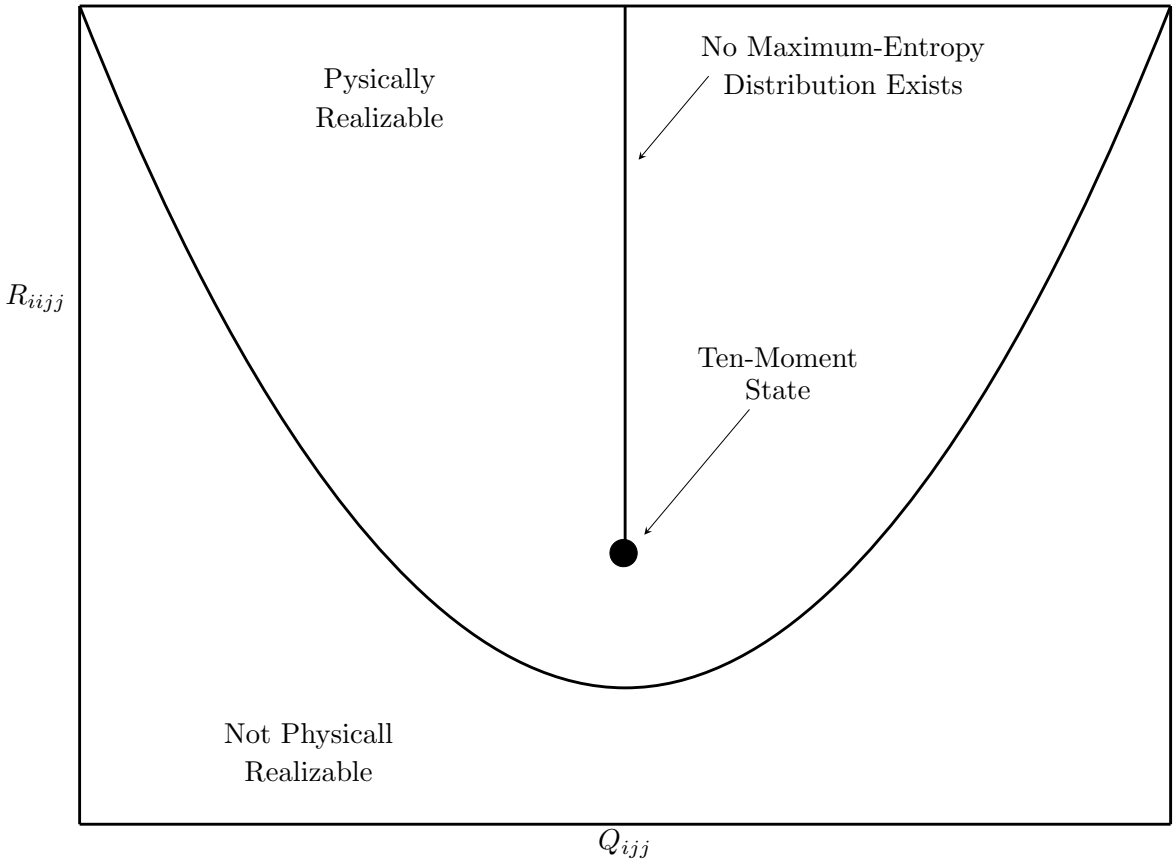

Figure 4.2: *Illustrative representation of the realizability region*

have the form

$$Q_{ijk} = K_{ijkm} Q_{mnn} \quad , \tag{4.3}$$

with

$$K_{ijkm} = \frac{\partial Q_{ijk}}{\partial Q_{mnn}} = [2P_{il}P^2_{jk} + 2P_{kl}P^2_{ij} + 2P_{jl}P^2_{ik}]B^{-1}_{lm} \quad , \tag{4.4}$$

and

$$B_{lm} = 2P_{lm}(P^2_{\alpha\alpha}) + 4(P^3_{lm}) \quad , \tag{4.5}$$

$$R_{ijkk} = \frac{1}{\sigma} Q_{ijl}(P^{-1})_{lm} Q_{mkk} + \frac{2(1-\sigma)P_{ik}P_{kj} + P_{ij}P_{kk}}{\rho} \quad , \tag{4.6}$$

and

$$S_{ijjkk} = \frac{1}{\sigma^2} P^{-1}_{kn} P^{-1}_{lm} Q_{npp} Q_{mjj} Q_{ikl} + 2\sigma^{\frac{1}{2}} \frac{P_{jj} Q_{ikk}}{\rho} + (1-\sigma^{\frac{1}{2}}) W_{im} Q_{mnn} \quad , \tag{4.7}$$

with

$$\begin{aligned} W_{im} = \left(\frac{1}{\rho}\right) & [2P_{il}\left(P_{\alpha\alpha}\right)^3 + 12P_{il}\left(P^3\right)_{\alpha\alpha} + \\ & 14\left(P^2\right)_{\alpha\alpha}\left(P^2\right)_{il} + 20\left(P^3\right)_{il} P_{\alpha\alpha} + \\ & 20\left(P^4\right)_{il} - 2\left(P^2\right)_{\alpha\alpha}\left(P\right)_{\beta\beta}\left(P\right)_{il} - \\ & 6\left(P\right)^2_{\alpha\alpha}\left(P^2\right)_{il}] B^{-1}_{lm} \end{aligned}$$

The resulting system of PDEs is very complex. It would be extremely difficult to evaluate the flux Jacobians. Certainly, no details of the eigenstructure of these matrices is known.

Chapter 5

Numerical Method

In this chapter, we present the details of the proposed method developed for the numerical computation of the solution of the governing partial differential equations outlined in Chapter 3 and 4. Section 5.1 describes the development of a Godunov-type finite-volume schemes. Section 5.2, reviews the Riemann problem and how to determine an approximate solution. This is used for inter-cellular flux evaluations. In Section 5.3, a brief review is given of the HLL approximate Riemann solver [10].

5.1 Godunov-Type Finite-Volume Methods

The numerical method used in the current study is based on Godunovs scheme [6], which has been considered by many scientists. Godunovs scheme can be derived from the integral form of the hyperbolic moment equations, which involve only first-order derivatives. The first step is to integrate the system of PDEs over an arbitrary cell in a computational mesh

$$\iiint_{V_i} \Big[\frac{\partial \mathbf{U}}{\partial t} + \vec{\nabla} \cdot \mathbf{F}\Big] dV = \iiint_{V_i} \mathbf{S} dV \,. \tag{5.1}$$

Where $\mathbf{U}$ is the conserved solution vector, $\mathbf{F}$ is the flux dyad and $\mathbf{S}$ is the source vector.

First, we separate the integral into two components, exchange the order of operations on the first term, and make use of the divergence theorem. Equation (5.1) can be rewritten, for the ith cell, as

$$\frac{d}{dt}\iiint_{V_i}\mathbf{U}dV+\oiint_{S_i}\mathbf{F}\cdot\hat{\mathbf{n}}dS=\iiint_{V_i}\mathbf{S}\,. \tag{5.2}$$

It is now clear that the rate of change of the conserved quantities, $\mathbf{U}$, in a control volume is dictated by the flux, $\mathbf{F}$, through the surface of the control volume and generation or destruction by the source vector. By realizing that $\frac{1}{V_i}\iiint_{V_i}\mathbf{U}dV=\bar{\mathbf{U}}$ is the average value of the conserved quantities in the control volume, Equation (5.2) can be rewritten as:

$$\frac{d\bar{\mathbf{U}}}{dt}=-\frac{1}{V_i}\oiint_{S_i}\mathbf{F}\cdot\hat{\mathbf{n}}dS+\frac{1}{V_i}\iiint_{V_i}\mathbf{S}\,. \tag{5.3}$$

When applied to a two-dimensional control volume in a mesh of quadrilaterals (as seen in Figure 5.1), and making use of explicit Euler time integration, Equation.(5.3) can be rewritten as:

$$\bar{\mathbf{U}}_i^{n+1}=\bar{\mathbf{U}}_i^n-\frac{\Delta t}{A_i}\left(\sum_k(\mathbf{F}_k\cdot n_k\;\Delta\ell)_k^n\right)+\Delta t\;\bar{\mathbf{S}}_i^n\,, \tag{5.4}$$

where A_i is the control volume area, $\hat{\mathbf{n}}$ is the outward-forcing unit normal to the k^{th} cell face and $\Delta\ell$ is the length of the k^{th} cell face. The superscript represents the index of the time step. The numerical fluxes at the faces of each cell, $(\mathbf{F}_k\cdot n_k\;\Delta\ell)$, are determined from the approximate solution of a Riemann problem. For this work, this is done using the HLL (Harten-Lax-van Leer) flux function. The distinguishing feature of Godunovs technique comes from the method through which the inter-cellular fluxes are determined. This is done through the solution of a Riemann problem, which automatically adds enough numerical dissipation to stabilize the scheme.

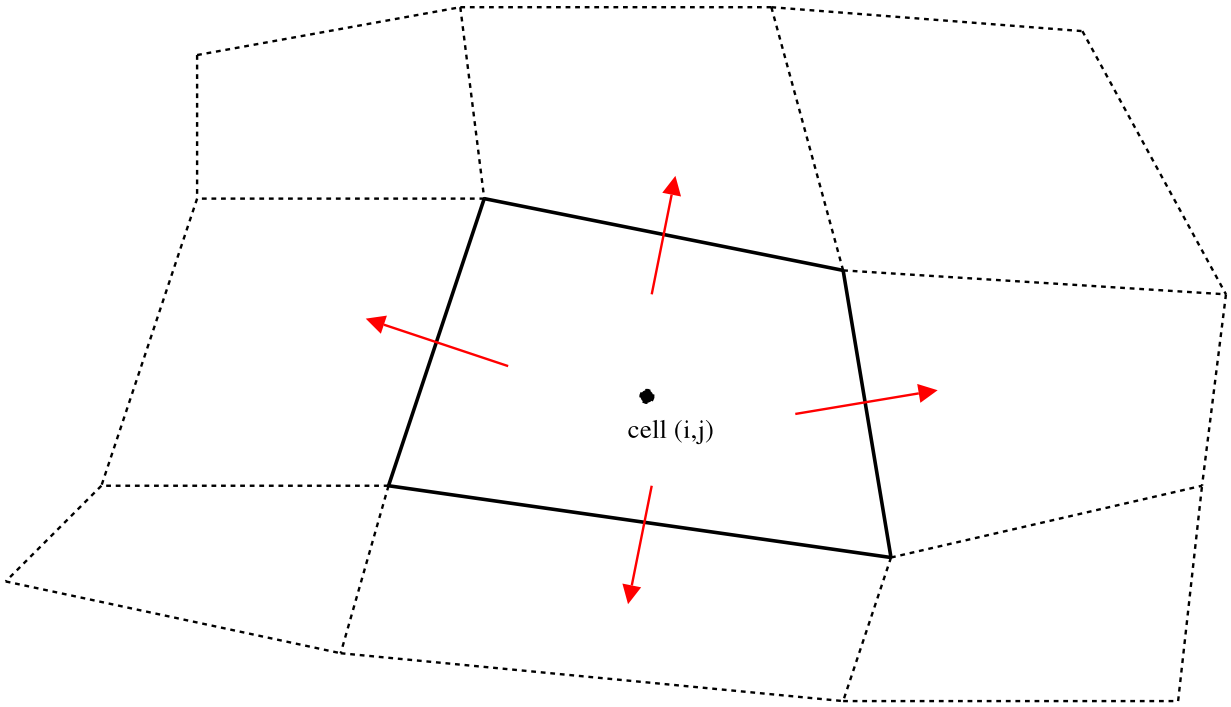

Figure 5.1: *Two-dimensional quadrilateral cell and inter-cellular fluxes*

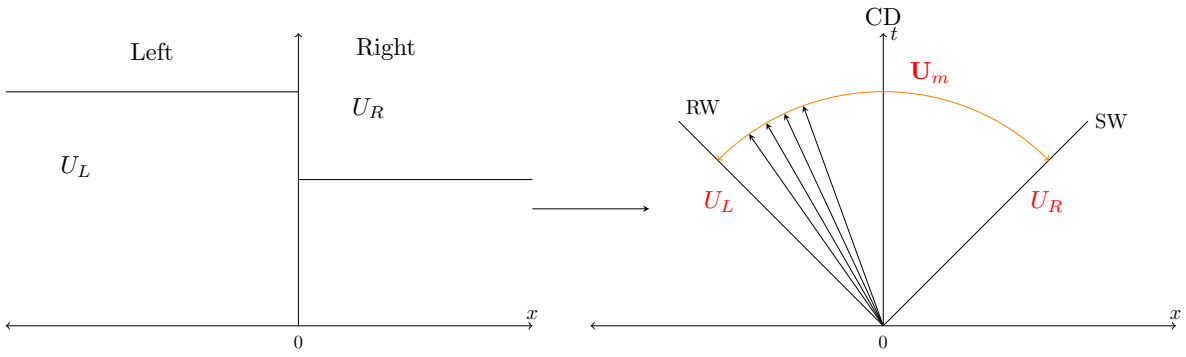

Figure 5.2: *Riemann Problem*

5.2 The Riemann Problem

The Riemann problem is a one-dimensional problem that demonstrates a hyperbolic systems response to a discontinuity. When formulated along the x axis, it has the following piece-wise constant initial data for the left and right states given by

$$\mathbf{U} = \begin{cases} U_{\mathrm{L}} & \text{if } x < x_0 \\ U_{\mathrm{R}} & \text{if } x \geq x_0 \end{cases}$$

As shown in Figure (5.2), for hyperbolic systems, this problem will have a self-similar solution and results in the generation of waves separating piecewise constant states. In Godunovs method the determination of the solution state at the cell interface is used to determine the flux between cells. For relatively simple equation sets, such as the Euler equations, exact Riemann solvers, such as the one proposed by Groth and Gottlieb [8], can be used. However, for more complicated systems, an exact solution is not available and approximate Riemann solvers must be used. In this work, the HLL approximate Riemann solver is used [10].

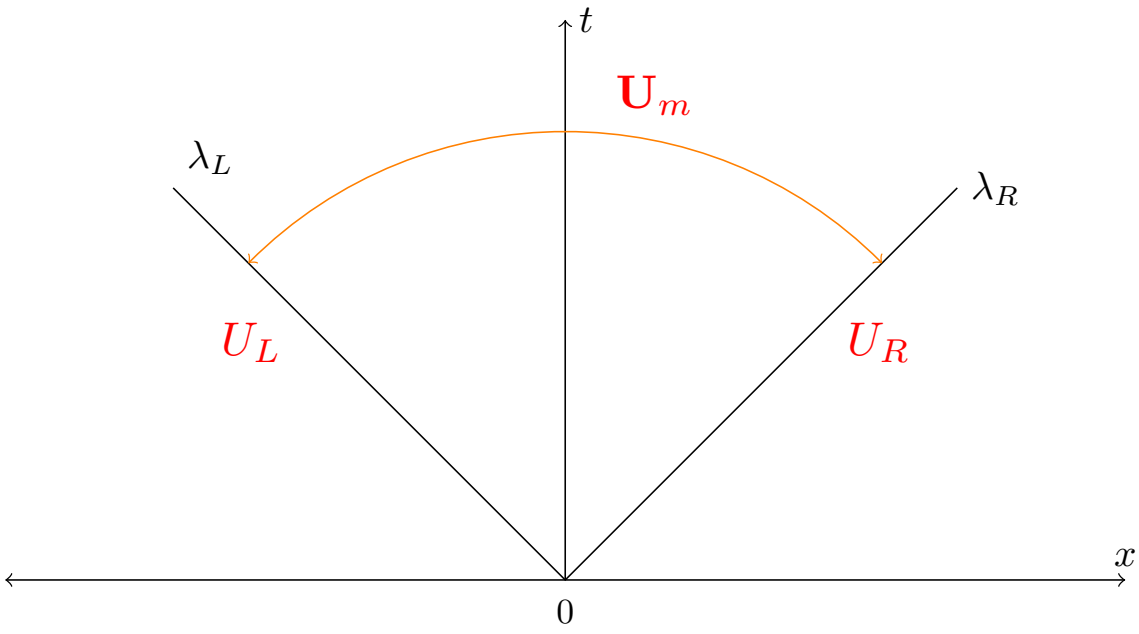

Figure 5.3: *Illustration of HLL approximate Riemann Solver*

5.3 The HLL Approximate Riemann Solver

In the approximate Riemann solver proposed by Harten, Lax and van Leer [10], the approximate Riemann solver can be derived from the one-dimensional conservation form of a hyperbolic set of equations (Greens theorem has been applied):

$$\oint_S (\mathbf{U}dx - \mathbf{F}dt) = 0\,. \tag{5.5}$$

As shown in Figure (5.3) it is assumed that, after the decay of the initial discontinuity of the local Riemann problem, only two waves propagate in two opposite directions with velocities λ_L and λ_R, generating a single state between them. Here, λ_L and λ_R are estimates of the smallest and the largest of the signal speeds arising from the solution of the Riemann problem. If a time step of Δt is taken, the left and right waves will have moved a distance

$\lambda_L \Delta t$ and $\lambda_R \Delta t$ respectively. Evaluating the path integral in Equation (5.5) gives:

$$-\mathbf{U}_L \lambda_L \Delta t + \mathbf{U}_R \lambda_R \Delta t - \mathbf{F}_R \Delta t - \mathbf{U}_m (\lambda_R - \lambda_L) \Delta t + \mathbf{F}_L \Delta t = 0\,. \tag{5.6}$$

Where where $\mathbf{F}_L$ and $\mathbf{F}_R$ are the Flux vectors evaluated at $\mathbf{U}_L$ and $\mathbf{U}_R$. This can be rearranged to give:

$$\mathbf{U}_m = \frac{\mathbf{U}_R \lambda_R - \mathbf{U}_L \lambda_L - (\mathbf{F}_R - \mathbf{F}_L)}{\lambda_R - \lambda_L}\,. \tag{5.7}$$

The goal of this approximate solver is to determine the flux at $x = 0$, or $\mathbf{F}_m$. Simply evaluating the flux at state $\mathbf{U}_m$, $\mathbf{F}(\mathbf{U}_m)$, will lead to a non-conservative scheme as Rankine-Hugoniot condition, $\Delta F = \lambda \Delta U$, will not be satisfied. The solution is to perform one more path integral. The new path integral comprises either the portion of the previous domain that is to the left or right of the $x = 0$ vertical line. If the left portion is chosen, this new integral yields:

$$-\mathbf{U}_L \lambda_L \Delta t - \mathbf{F}_m \Delta t + \mathbf{U}_m \lambda_L \Delta t + \mathbf{F}_L \Delta t = 0\,. \tag{5.8}$$

This can be rearranged to give:

$$\mathbf{F}_m = \mathbf{F}_L + \lambda_L (\mathbf{U}_m - \mathbf{U}_L)\,, \tag{5.9}$$

by substituting this in Equation (5.8), we have

$$\mathbf{F}_m = \frac{\mathbf{F}_L \lambda_R - \mathbf{F}_R \lambda_L + (\mathbf{U}_R - \mathbf{U}_L)(\lambda_R \lambda_L)}{\lambda_R - \lambda_L}\,. \tag{5.10}$$

Evaluating a path around the right-hand portion of the region will yield an identical result. Lastly, the two wave speeds must be determined. The wave speed λ_R is taken to be the maximum wave speed of $\mathbf{U}_R$, and λ_L is the minimum wave speed of $\mathbf{U}_L$. The final HLL

flux function is given by:

$$\mathbf{F} = \begin{cases} \mathbf{F_L} & \text{if } \lambda_L > 0 \\ \mathbf{F_m} & \text{if } \lambda_L < 0 \ \& \ \lambda_R > 0 \\ \mathbf{F_R} & \text{if } \lambda_R < 0 \end{cases}$$

5.4 Explicit-Euler time marching

As stated earlier, the explicit Euler time marching scheme has been used in this work.. This time-marching method is widely used for solving steady and unsteady flows problems in computational fluid dynamics. It tend to be easy to implement and code. Explicit methods use the state of the system at the current time in order to calculate an update to find the state of the system at a later time as given:

$$\mathbf{U}^{n+1} = \mathbf{U}^n + \triangle t R^n \,, \tag{5.11}$$

where $R = \frac{d\mathbf{U}}{dt}$.

In order to ensure stability of this explicit method, the time step can be no longer than

$$\Delta t = \frac{\Delta x}{\max(|\lambda|)} \,,$$

where Δx is the grid spacing and $\max(|\lambda|)$ is the largest absolute value of any wave speed. A CFL (Courant-Friedrich-Lavy) number is defined as a safety factor such that the actual time step used is

$$\Delta t = \mathrm{CFL}\frac{\Delta x}{\max(|\lambda|)} \,.$$

Chapter 6

Results

Three situations are chosen that demonstrate the advantages of a fourteen moment description as compared to previous methods. For each situation, we try to solve the problem using each of the models discussed in the previous chapters. First, we consider two crossing beams of non-interacting particles. Single-velocity descriptions are incapable of describing such crossing of particle trajectories. Second, a situation of one group of fast-moving particles which overtakes and passes through a group of slower particles is considered. Third, two crossing beams of non-interacting particles with a background acceleration field, meant to represent a drag force, is treated. In all these cases, much of the domain contains no particles. Numerical errors can result in some areas developing non-physical states especially for the fourteen moment description. For example, in some regions, where the density should be zero, numerical errors can result in a very small negative value. It is therefore necessary to ensure the state in each cell is realizable after each time step. For any cells that have states that are slightly out of a realizable state, one simply moves back to the boundary of realizability before the next time step. A CFL number of 0.5 was used in all cases.

6.1 Crossing Beams

In order to verify and explore the accuracy of the different models, the first case considered is that of two crossing jets of particles in a vacuum. For this case, a mesh of 600 by 600 cells is used. This yields meshes of 360,000 equally sized cells. The domain is $0.0\,\mathrm{m} < x < 2.0\,\mathrm{m}$ and $-1.0\,\mathrm{m} < y < 1.0\,\mathrm{m}$. The boundary conditions are transmissive everywhere except on the left boundary, where two jets of particles enter. If $-0.8\,\mathrm{m} < y < -0.6\,\mathrm{m}$ on this wall, a jet of particles, all with $\rho = 1\,\mathrm{kg/m^3}$, $u_x = 1\,\mathrm{m/s}$, and $u_y = 1\,\mathrm{m/s}$, enters. If $0.6\,\mathrm{m} < y < 0.8\,\mathrm{m}$ another jet of particles with $\rho = 1\,\mathrm{kg/m^3}$, $u_x = 1\,\mathrm{m/s}$, and $u_y = -1\,\mathrm{m/s}$ enters. Solutions were advanced in time until steady-state was reliably achieved. As the particles are assumed not to interact with each other, the exact solution is that the two beams should continue in straight lines and exit the domain, as shown in Figure 6.1. Computed solutions for particle density when a single-velocity model is used are shown in Figures 6.2, the beams cannot cross and the particles simply clump together along the symmetry line. This popular method is completely inappropriate for this situation. In the Euler-model solutions, shown in Figures 6.3, the beams cannot cross and we can see the presence of shock waves after the intersection point. A dispense cloud of particles expands into the vacuum. For the Gaussian model solutions, shown in Figures 6.4, the beams do appears to start crossing each other. However, the results are not very clear. The fourteen moment solutions, shown in Figures 6.5, correctly allows the beams to cross. However, following the crossing, the beams expand and dissipate. It is thought that this is largely due to numerical dissipation. Certainly, no model is able to reproduce the exact solution to high accuracy. It is clear that each time the complexity of the model is increased, the

quality of solution improves.

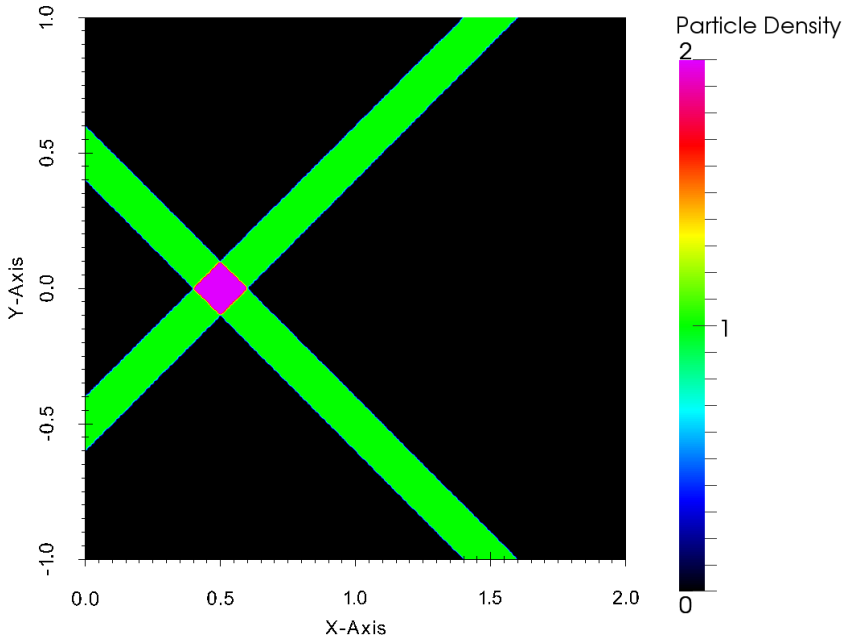

Figure 6.1: *Illustration of the exact solution, crossing beams*

6.2 Superimposed Families of Particles

The second case considered is that of one family of non-interacting particles overtaking another. For this case, a mesh of 600 by 600 cells is used. This yields meshes of 360,000 equally sized cells. In this case, at time zero, one family of particles with $\rho = 1\,\mathrm{kg/m^3}$ and $u_x = 1\,\mathrm{m/s}$ spans the region $1.0\,\mathrm{m} < x < 1.4\,\mathrm{m}$ and $0.5\,\mathrm{m} < y < 1.5\,\mathrm{m}$. A second family with $\rho = 1\,\mathrm{kg/m^3}$ and $u_x = 6.0\,\mathrm{m/s}$ spans the region $0.4\,\mathrm{m} < x < 0.6\,\mathrm{m}$ and $0.8\,\mathrm{m} < y < 1.2\,\mathrm{m}$. Results at $t = 0s$, $t = 0.1\,\mathrm{s}$, $t = 0.2\,\mathrm{s}$, $t = 0.3\,\mathrm{s}$, $t = 0.4\,\mathrm{s}$ and $t = 0.6\,\mathrm{s}$ are shown in Figure 6.6. Again, the exact solution should show the faster family of particles simply passing through the slower one, completely unaffected. As shown in Figure 6.7, it can again be seen that the single-velocity model is wholly unable to predict this effect as particles again collect in a concentrated region. Similarly, in the Euler model solutions,

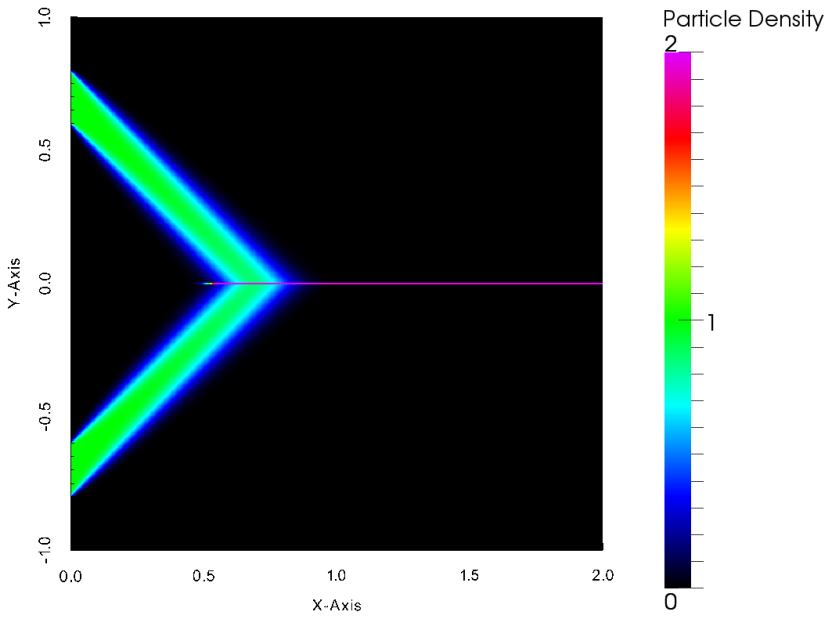

Figure 6.2: *Solution for case of two crossing beams of non-interacting particles, computed using the single-velocity model.*

shown in Figures 6.8, the faster family of particles is unable to keep its shape after moving through the second family. For the Gaussian model solutions, shown in Figures 6.9, we have better results than the two previous models. However, the particles from the region of interaction quickly dissipate. The results for the fourteen-moment formulation, as shown in Figure 6.10 are not much better. It can be seen that the faster particles do pass through the slower group, however, there is a noticeable interaction. It is thought at this time that this is largely due to numerical errors incurred when the two families initially come in contact with each other. It is possible that this due to our choice of the numerical method. Further study of this process is needed.

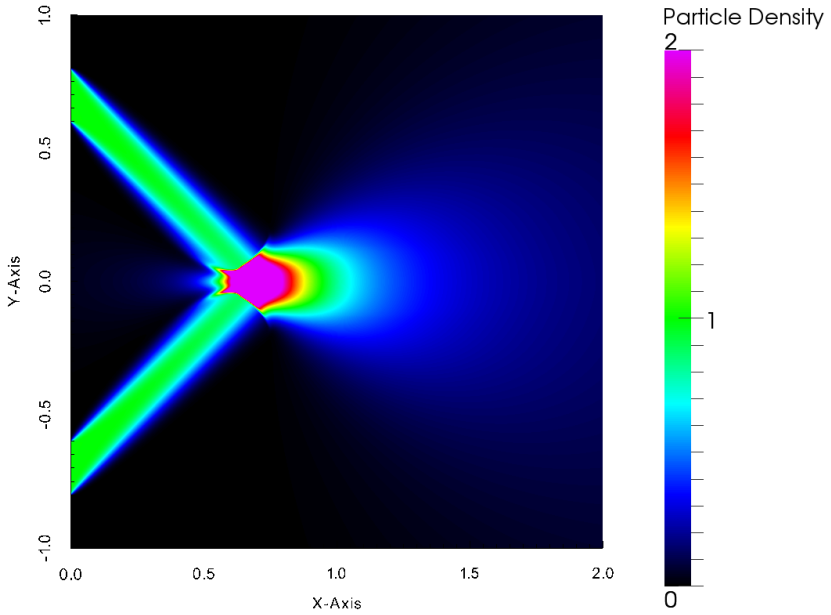

Figure 6.3: *Solutions for case of two crossing beams of non-interacting particles, computed using the Euler model*

6.3 Crossing Beams with Acceleration Field

The final case considered is that of two jets of particles in an imposed background flow field. Specifically, the domain stretches from $0.0\,\mathrm{m} < x < 3.0\,\mathrm{m}$ and $-0.75\,\mathrm{m} < y < 0.75\,\mathrm{m}$. On the left boundary, when $-0.6\,\mathrm{m} < y < -0.4\,\mathrm{m}$ or $0.4\,\mathrm{m} < y < 0.6\,\mathrm{m}$, particles enter with $\rho = 1\,\mathrm{kg/m^3}$, $u_x = 0.2\,\mathrm{m/s}$, and $u_y = 0.0\,\mathrm{m/s}$. For this case, we fix $\tau = 8.0\,\mathrm{s}$. There exists an imposed velocity of a background fluid of the form

$$\left\{ \begin{array}{l} u_{gx} = 0.2\,\mathrm{m/s} \\ u_{gy} = -\varepsilon y \end{array} \right\}$$

Here, ε is taken to be $2.5\,\mathrm{s^{-1}}$. This situation is similar to one studied previously [30] and is chosen because an exact solution can be constructed.

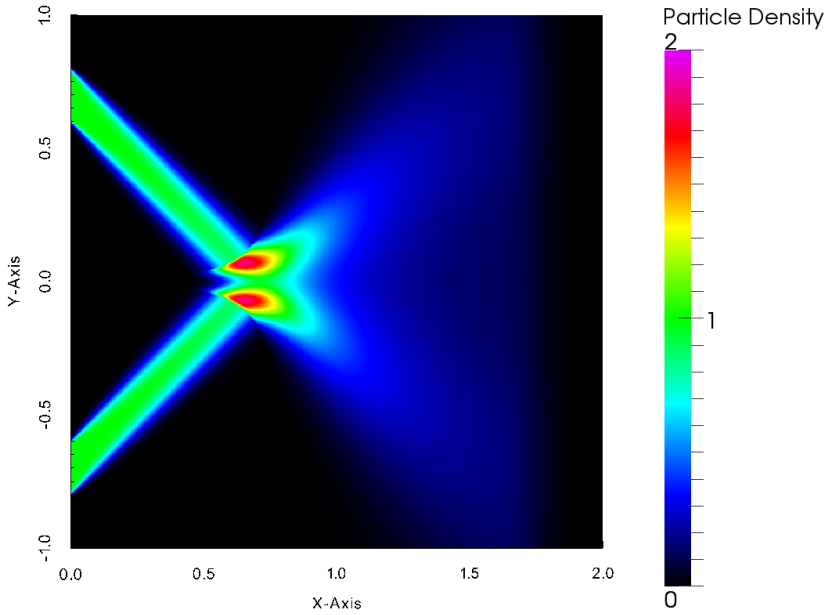

Figure 6.4: *Solution for case of two crossing beams of non-interacting particles, computed using the Gaussian model.*

6.3.1 Exact solution

The exact solution can be obtained by integrating the Lagrangian equations for any particle, starting at $x = 0$ with velocity $u_{px} = 0.2\,\mathrm{m/s}$ and $u_{py} = 0\,\mathrm{m/s}$. The ordinary differential equations describing this situation are

$$\frac{\mathrm{d}y_p}{\mathrm{d}t} = u_y, \frac{\mathrm{d}u_y}{\mathrm{d}t} = \frac{-1}{\tau_p}(u_y - v_g(y)) = \frac{-1}{\tau_p}(u_p + \varepsilon y)$$

where y_P is the y coordinate of the particle. Combining the Lagrangian equations yields a scalar second order equation that describes the y motion in a frame that moves along the x axis with the particle's x-direction velocity, u_x,

$$\frac{\mathrm{d}y^2}{\mathrm{d}t^2} + \frac{1}{\tau}\frac{\mathrm{d}y}{\mathrm{d}t} + \frac{\varepsilon}{\tau_p}y = 0$$

Assuming a Stokes flow, we define a Stokes number $\mathrm{St} = \varepsilon\tau_p$ and $\omega^2 = \frac{1}{4}|\frac{1}{\tau_p^2} - \frac{4\varepsilon}{\tau_p^2}|$. This

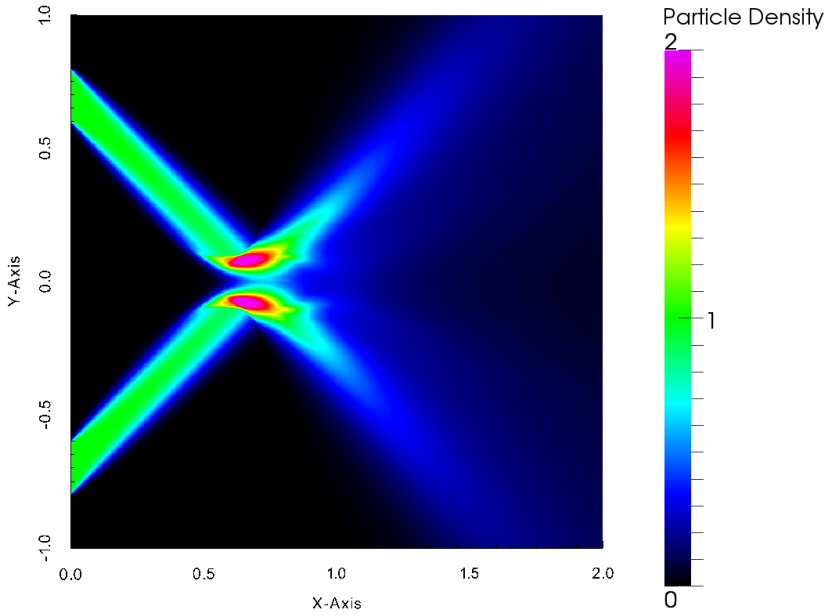

Figure 6.5: *Solution for case of two crossing beams of non-interacting particles, computed using the Fourteen-moment model.*

system has a critical Stokes number, $\mathrm{St}_c = \frac{1}{4}$, above which the solution is oscillatory.

$$Y_p(t) = y_0 \exp(-\frac{1}{2\tau_\mathrm{p}}) = \begin{cases} \exp(-\omega \mathrm{t}) & \text{if } \mathrm{St} < \frac{1}{4} \\ \cos(-\omega t) + \frac{1}{2\omega\tau_p}\sin(-2\omega t) & \text{Otherwise} \end{cases}$$

This is shown graphically in Figure 6.11.

6.3.2 Eulerian Model Solutions

In this final case, we have two crossing beams of non-interacting particles with an imposed background velocity field that generates a drag force. For this case, a mesh of 1000 by 200 cells is used. This yields meshes of 200,000 equally sized cells. In this case, the domain is $0.0\,\mathrm{m} < x < 3.0\,\mathrm{m}$ and $-0.75\,\mathrm{m} < y < 0.75\,\mathrm{m}$. The boundary conditions are transmissive everywhere except on the left boundary, where two jets of particles enter. If $-0.6\,\mathrm{m} < y < -0.4\,\mathrm{m}$ on this wall, a jet of particles, all with $\rho = 1.0\,\mathrm{kg/m^3}$, $u_x = 0.2\,\mathrm{m/s}$,

and $u_y = 0.0\,\mathrm{m/s}$, enters. If $0.4\,\mathrm{m} < y < 0.6\,\mathrm{m}$ another jet of particles with $\rho = 1.0\,\mathrm{kg/m^3}$, $u_x = 0.2\,\mathrm{m/s}$, and $u_y = 0.0\,\mathrm{m/s}$ enters. Results obtained using the single-velocity model are shown in Figures 6.12, again the beams cannot cross. For the Euler model solutions, shown in Figures 6.13, the beams cannot cross and we can see the presence of a shock wave after the intersection point. This leads to a complex structure in the model solution that is very different from the true solution. For the Gaussian model solutions, shown in Figures 6.14, the particle beams do cross. This is surprising, as this case was previously investigated by Vie et al. [30] using the Gaussian model, and no crossing was observed. A different numerical method was used in their case, and the current results seem far closer to the desired solution. For the 14-moment model, shown in Figure 6.15, the jets also cross once. The results are very similar to the 10-moment case. This is surprising, as it was expected that the bi-modal distribution of the 14-moment model would be needed to achieve such a crossing.

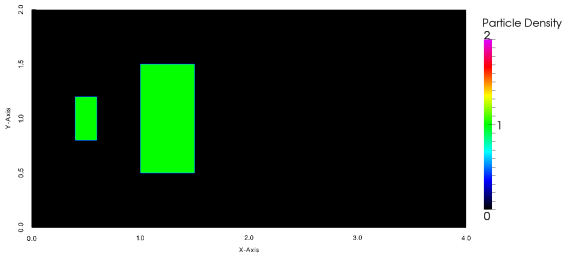

(a) *Exact solution,* $t = 0.0\,\mathrm{s}$

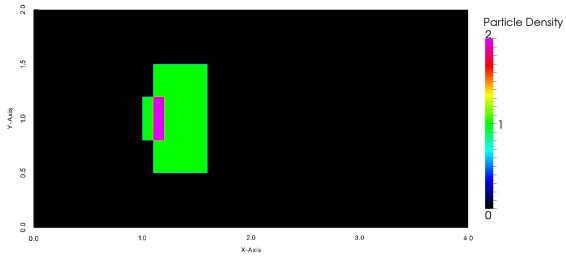

(b) *Exact solution,* $t = 0.1\,\mathrm{s}$

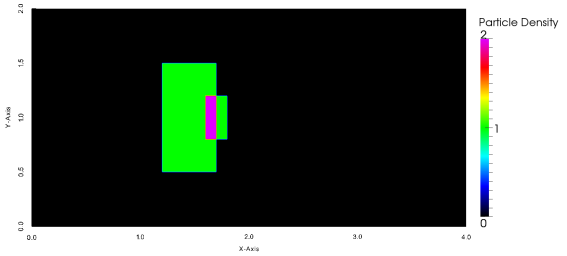

(c) *Exact solution,* $t = 0.2\,\mathrm{s}$

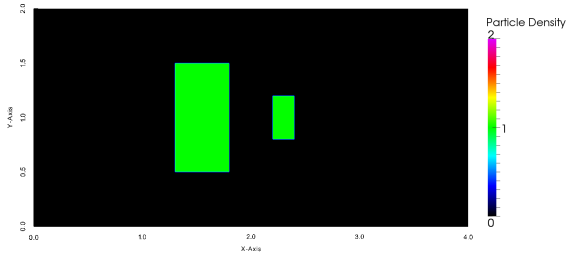

(d) *Exact solution,* $t = 0.30\,\mathrm{s}$

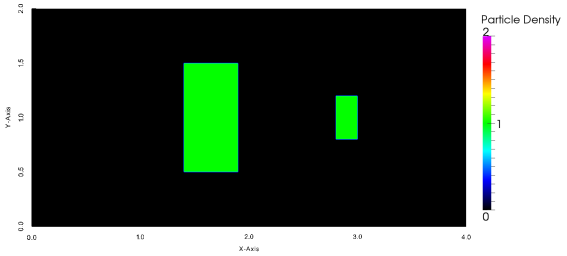

(e) *Exact solution,* $t = 0.40\,\mathrm{s}$

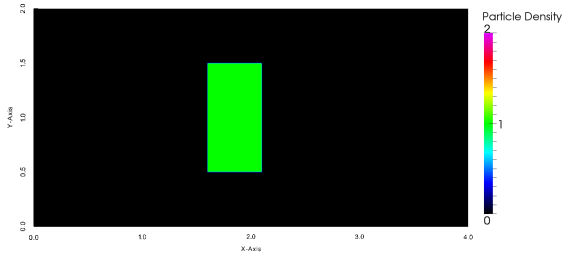

(f) *Exact solution,* $t = 0.6\,\mathrm{s}$

Figure 6.6: *Solutions for case of one family of non-interacting particles overtaking another, Exact solution.*

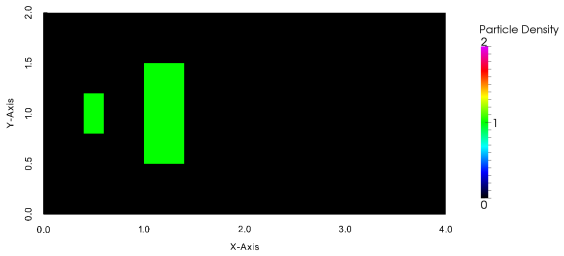

(a) *Single-velocity model,* $t = 0.0\,\mathrm{s}$

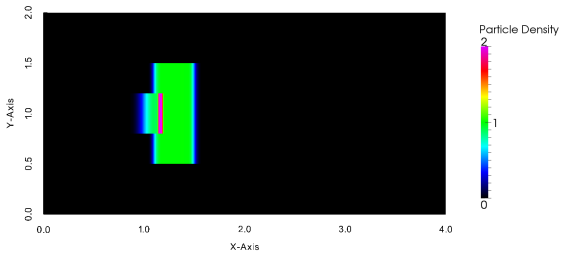

(b) *Single-velocity model,* $t = 0.1\,\mathrm{s}$

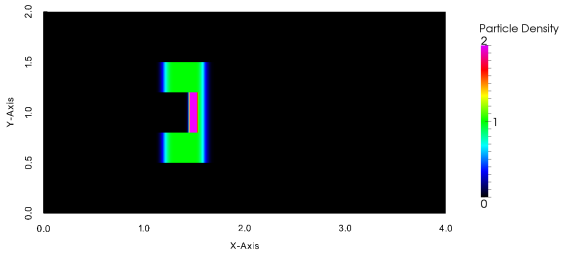

(c) *Single-velocity model,* $t = 0.2\,\mathrm{s}$

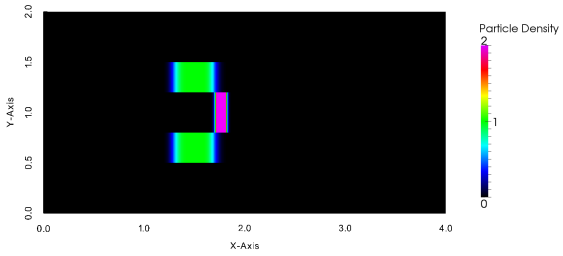

(d) *Single-velocity model,* $t = 0.30\,\mathrm{s}$

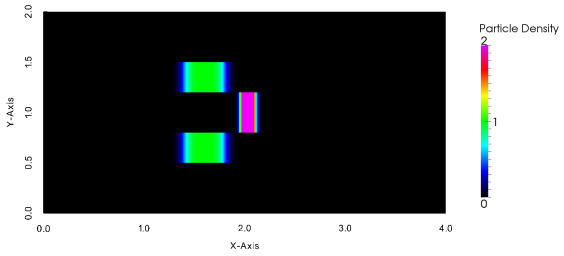

(e) *Single-velocity model,* $t = 0.40\,\mathrm{s}$

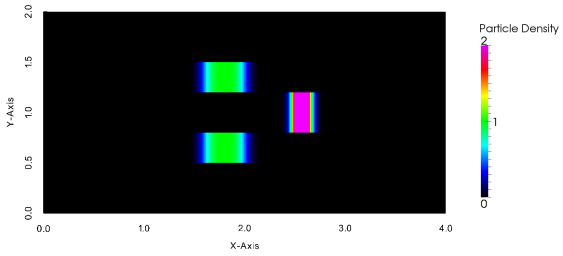

(f) *Single-velocity model,* $t = 0.6\,\mathrm{s}$

Figure 6.7: *Solutions for case of one family of non-interacting particles overtaking another, computed using single-velocity model.*

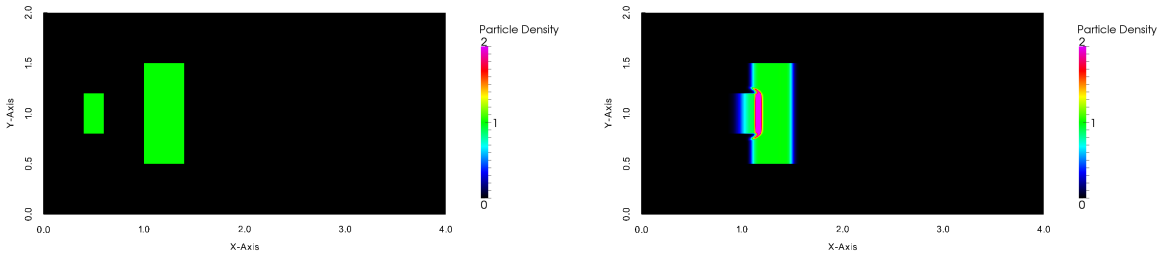

(a) *Euler model*, $t = 0.0\,\mathrm{s}$

(b) *Euler model*, $t = 0.1\,\mathrm{s}$

(c) *Euler model*, $t = 0.20\,\mathrm{s}$

(d) *Euler model*, $t = 0.30\,\mathrm{s}$

(e) *Euler model*, $t = 0.40\,\mathrm{s}$

(f) *Euler model*, $t = 0.6\,\mathrm{s}$

Figure 6.8: *Solutions for case of one family of non-interacting particles overtaking another, computed using Euler model.*

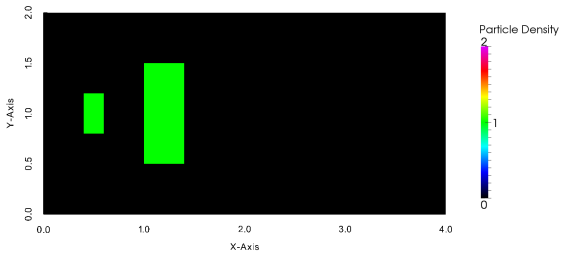

(a) *Gaussian model,* $t = 0.0\,\mathrm{s}$

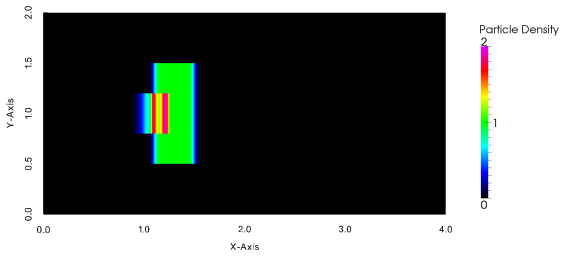

(b) *Gaussian model,* $t = 0.1\,\mathrm{s}$

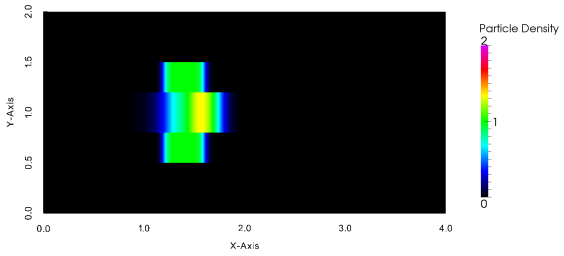

(c) *Gaussian model,* $t = 0.20\,\mathrm{s}$

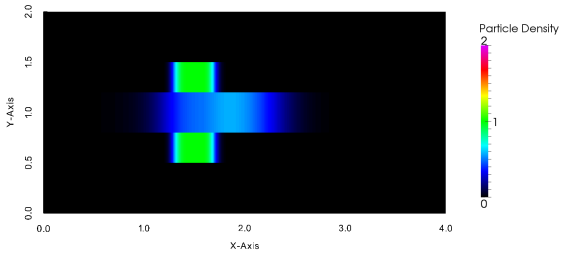

(d) *Gaussian model,* $t = 0.30\,\mathrm{s}$

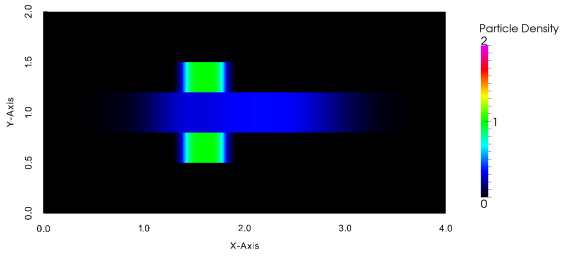

(e) *Gaussian model,* $t = 0.40\,\mathrm{s}$

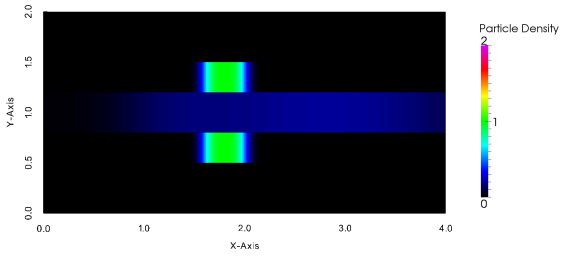

(f) *Gaussian model,* $t = 0.6\,\mathrm{s}$

Figure 6.9: *Solutions for case of one family of non-interacting particles overtaking another, computed using Gaussian model.*

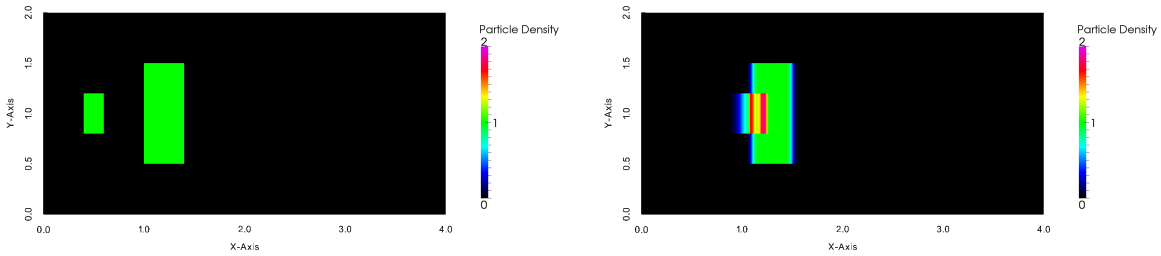

(a) *Fourteen-moment model,* $t = 0.0\,\mathrm{s}$

(b) *Fourteen-moment model,* $t = 0.1\,\mathrm{s}$

(c) *Fourteen-moment model,* $t = 0.2\,\mathrm{s}$

(d) *Fourteen-moment model,* $t = 0.30\,\mathrm{s}$

(e) *Fourteen-moment model,* $t = 0.40\,\mathrm{s}$

(f) *Fourteen moment model,* $t = 0.6\,\mathrm{s}$

Figure 6.10: *Solutions for case of one family of non-interacting particles overtaking another, computed using the fourteen-moment model.*

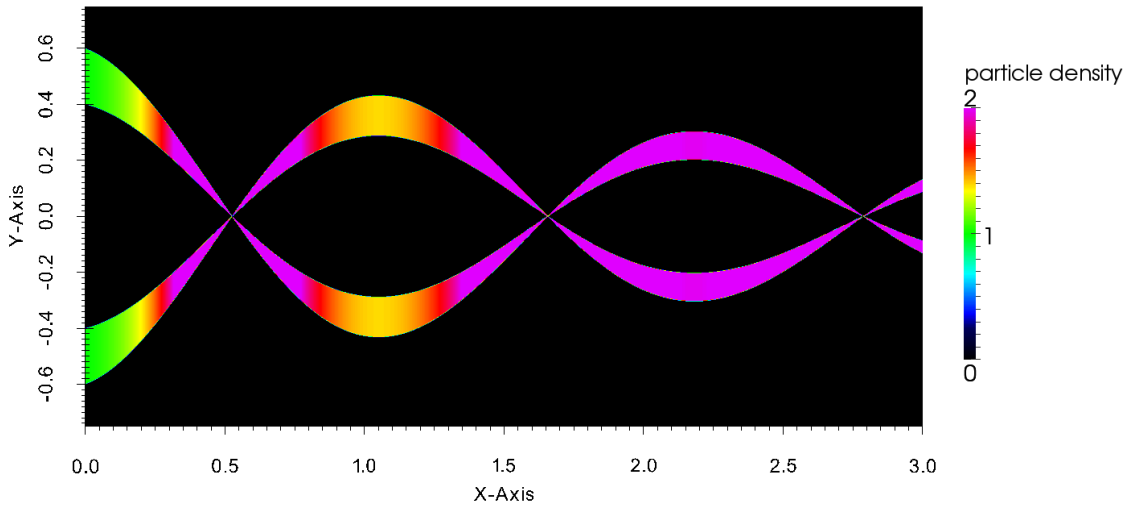

Figure 6.11: *Steady solution of two inertial particle jets (St = 8.0) injected in a compressive velocity field: particle number density*

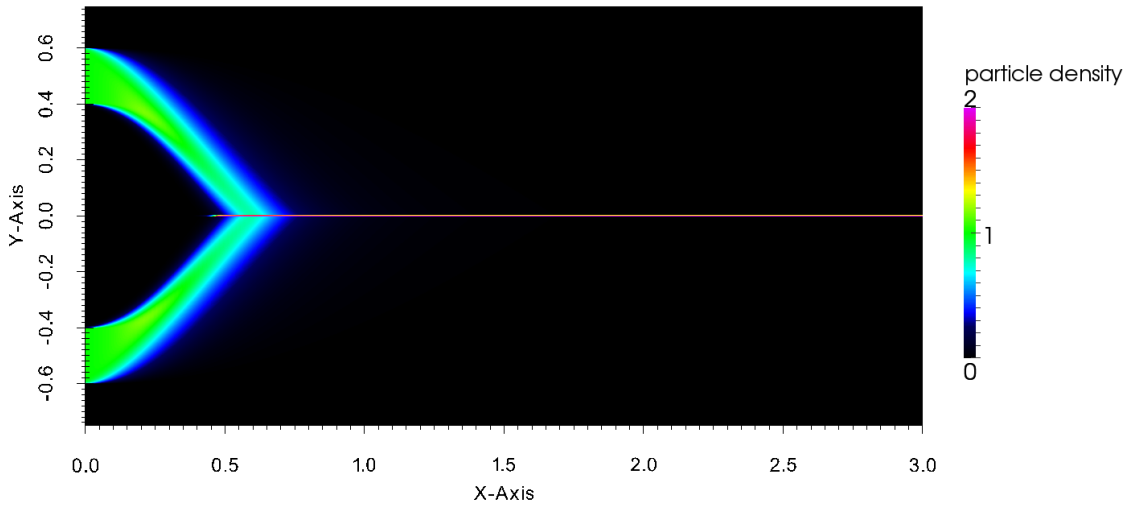

Figure 6.12: *Single-velocity model, particle density*

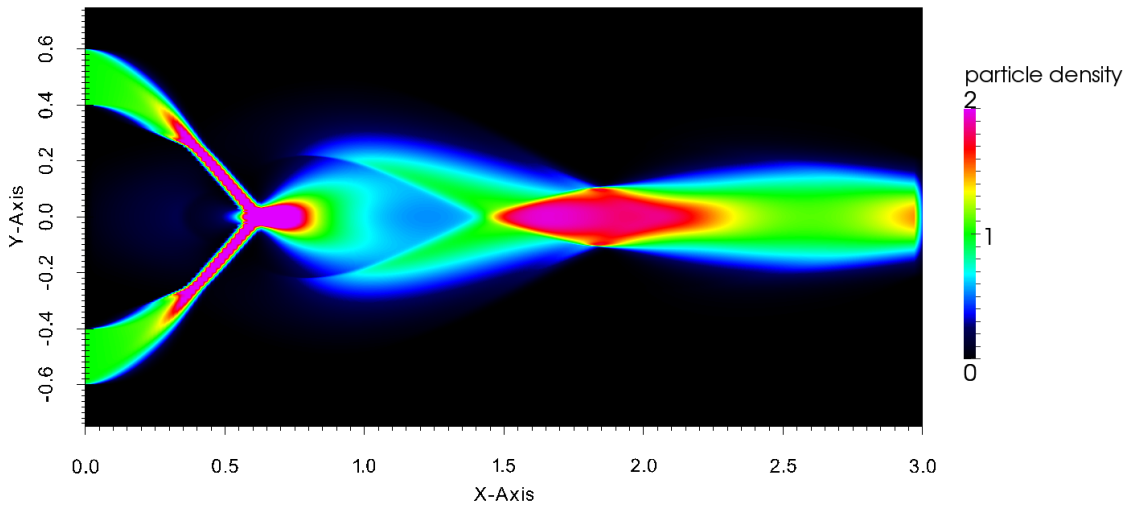

Figure 6.13: *Euler model, particle density*

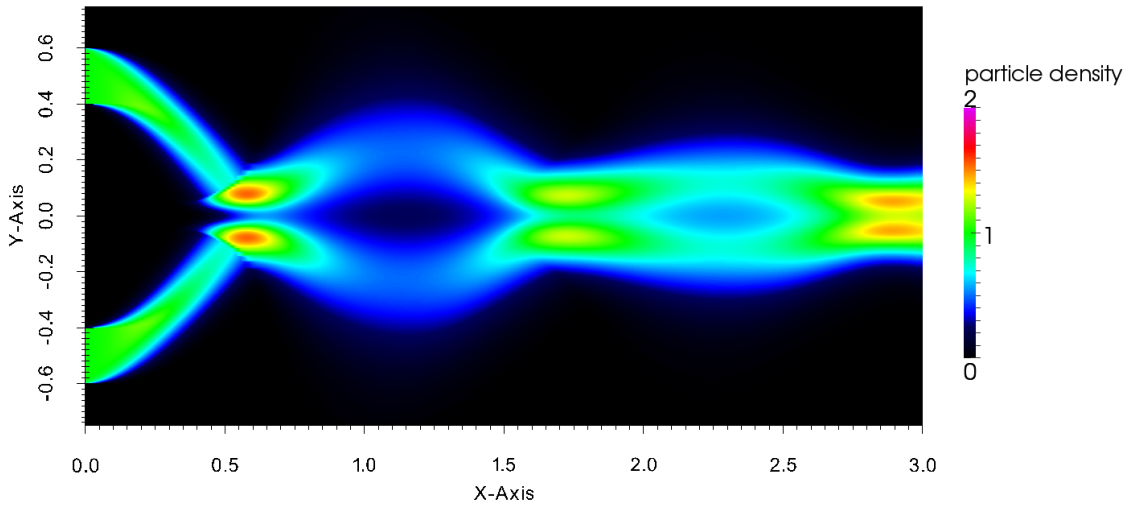

Figure 6.14: *Gaussian model, particle density*

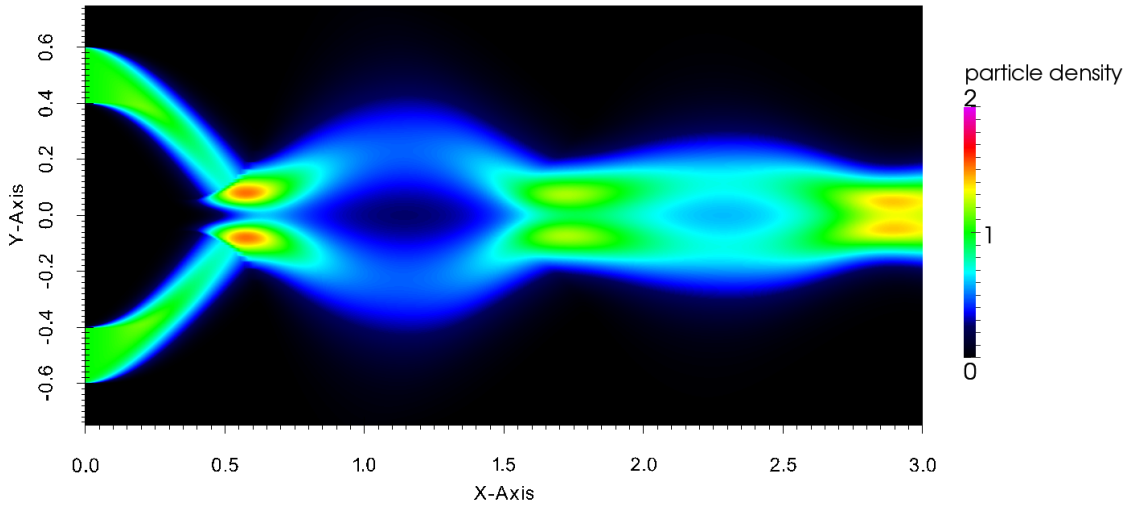

Figure 6.15: *Fourteen-moment model, particle density*

Chapter 7

Conclusions

This research entailed the investigation of novel models for an inert, dilute, disperse, particle flow, possibly coupled to a background fluid flow. Such flows are important in many engineering situations. Particle phases are often difficult to model, as Lagrangian methods can be too costly and many Eulerian methods suffer from severe model deficiencies and mathematical artifacts. This work examines and compares several multi-velocity formulations for the prediction of gas-particle flows. In a quest for new multi-velocity treatments for particle-gas flows that eliminate some or all of the artifacts of previous treatments while maintaining desirable mathematical structures (such as Galilean invariance), it has been demonstrated that the higher-order moment-closure-based model offers many advantages when compared to the single-velocity, or five-moment treatments. The use of such models has shown to provide Eulerian models with the potential for the prediction of crossing streams of particles. If there are two or more groups of intersecting particles, particle crossing is impossible in the single-velocity, or Euler model. Thus, higher-order models have the promise of being more physically accurate in situations when particles at a given location and time do not all have the same (or nearly the same) velocity. It is hoped that these mod-

els provide a good balance of improved physical accuracy over the standard, single-velocity treatment, while remaining less costly than the more expensive multi-velocity treatments where the distribution of particle velocities must be computed using a costly algorithm for every flux evaluation. The goal of this work that should be taken from this study into higher-order moment systems is that there do exist higher-order moment closures and techniques that can be used to obtain a closed system for highly non-equilibrium flow problems, such as the crossing beams case. It was shown that the fourteen-moment model produce superior results for coupling of the particle model to a fluid model for a background gas flow. The field of gaskinetic theory provides a framework for this coupling through the acceleration term. Finally, numerical solutions for several canonical and traditionally difficult flow situations was shown for each method and comparisons was made.

7.1 Suggestion and Future Work

It is clearly demonstrated that the idea of using the fourteen moment model to solve the multi-phase problems is better than the other models. The numerical methods used in this thesis were only first-order accurate. Higher-order methods should allow a higher resolution of solution details and may reveal previously unseen effects. Non-interacting particles were used in this work, as this is the most difficult case to model. Real particles, however, do interact. For the application of these models to real situations, an appropriate collision operator is needed. Once again, gaskinetic theory offers a mature theory for this, but the details of construction remain to be worked out and likely depend on the situation.

References

[1] S. L. Brown. *Approximate Riemann Solvers for Moment Models of Dilute Gases*. PhD thesis, University of Michigan, 1996.

[2] S. L. Brown, P. L. Roe, and C. P. T. Groth. Numerical solution of a 10-moment model for nonequilibrium gasdynamics. Paper 95-1677, AIAA, June 1995.

[3] J. M. Burgers. *Flow Equations for Composite Gases*. Academic Press, New York, 1969.

[4] S. Chapman and T. G. Cowling. *The Mathematical Theory of Non-Uniform Gases*. Cambridge University Press, Cambridge, 1960.

[5] R. O. Fox. Higher-order quadrature-based moment methods for kinetic equations. *J. Comput. Phys.*, 228:7771–7791, 2009.

[6] S. K. Godunov. Finite-difference method for numerical computations of discontinuous solutions of the equations of fluid dynamics. *Mat. Sb.*, 47:271–306, 1959.

[7] T. I. Gombosi. *Gaskinetic Theory*. Cambridge University Press, Cambridge, 1994.

[8] J. J. Gottlieb and C. P. T. Groth. Assessment of Riemann solvers for unsteady one-dimensional inviscid flows of perfect gases. *J. Comput. Phys.*, 78:437–458, 1988.

[9] H. Grad. On the kinetic theory of rarefied gases. *Commun. Pure Appl. Math.*, 2:331–407, 1949.

[10] A. Harten, P. D. Lax, and B. van Leer. On upstream differencing and Godunov-type schemes for hyperbolic conservation laws. *SIAM Rev.*, 25(1):35–61, 1983.

[11] F. Hertweck. Allgemeine 13-momenten-näherung zur fokker-planck-gleichung eines plasmas. *Zeitschrift für Naturforschung*, 20a:1243–1255, 1965.

[12] L. H. Holway, Jr. *Approximation Procedures for Kinetic Theory.* PhD thesis, Harvard University, 1963.

[13] L. H. Holway, Jr. Kinetic theory of shock structure using an ellipsoidal distribution function. In J. H. e Leeuw, editor, *Rarefied Gas Dynamics*, volume I, pages 193–215, New York, 1966. Academic Press.

[14] L. H. Holway, Jr. New statistical models for kinetic theory: Methods of construction. *Phys. Fluids*, 9(9):1658–1673, 1966.

[15] L. H. Holway, Jr. The effect of collisional models upon shock wave structure. In C. L. Brundin, editor, *Rarefied Gas Dynamics*, volume I, pages 759–784, New York, 1967. Academic Press.

[16] M. Junk. Domain of definition of Levermore's five-moment system. *J. Stat. Phys.*, 93(5/6):1143–1167, 1998.

[17] C. D. Levermore. Moment closure hierarchies for kinetic theories. *J. Stat. Phys.*, 83:1021–1065, 1996.

[18] C. D. Levermore and W. J. Morokoff. The Gaussian moment closure for gas dynamics. *SIAM J. Appl. Math.*, 59(1):72–96, 1998.

[19] J. C. Maxwell. On the dynamical theory of gases. *Philosophical Transactions of the Royal Society of London*, 157:49–88, 1867.

[20] J. G. McDonald and C. P. T. Groth. Towards realizable hyperbolic moment closures for viscous heat-conducting gas flows based on a maximum-entropy distribution. *Continuum Mech. Thermodyn.*, 25:573–603, 2013.

[21] J. G. McDonald and M. Torrilhon. Affordable robust moment closures for CFD based on the maximum-entropy hierarchy. *J. Comput. Phys.*, 251:500–523, 2013.

[22] I. Müller and T. Ruggeri. *Rational Extended Thermodynamics*. Springer-Verlag, New York, 1998.

[23] O.Desjardins, R.O. Fox, and P.Villedieu. A quadrature-based moment method for dilute fluid-particle flows. *J. Comput. Phys.*, 227:2514–2539, 2008.

[24] V. Oraevskii, R. Chodura, and W. Feneberg. Hydrodynamic equations for plasmas in strong magnetic fields — I collisionless approximation. *Plasma Phys.*, 10:819–828, 1968.

[25] N. Raju and E.Maiburg. The accumulation and dispersion of heavy particles in forced two-dimensional mixing layers.part 2:the effect of gravity. *Phys. Fluids*, 7:1241–1264, 1995.

[26] J. S. Sachdev. *Parallel Solution-Adaptive Method for Predicting Solid Propellant Rocket Motor Core Flows*. PhD thesis, University of Toronto, April 2007.

[27] J. S. Sachdev, C. P. T. Groth, and J. J. Gottlieb. Numerical solution scheme for inert, disperse, and dilute gas-particle flows. *International Journal of Multiphase Flow*, 33:282–299, 2007.

[28] R. Saurel, E. Daniel, and J. C. Loraud. Two-phase flows: Second-order schemes and boundary conditions. *AIAA J.*, 32(6):1214–1221, June 1994.

[29] S. A. Slater and J. B. Young. The calculation of inertial particle transport in dilute gas-particle flows. *Int. J. Multiphase Flow*, 27:61–87, 2001.

[30] A. Vie, F. Doisneau, and M. Massot. On the anisotropic gaussian velocity closure for inertial-particle laden flows. *Commun. Comput. Phys.*, 17:1– 46, 2015.

[31] T. L. Wen, F.Yang, Y. Crowe, C. T. Chung, and J. N.Troutt. Self-organizing particle dispersion mechanism in a plane wake. *Phys. Fluids*, pages 301–318, 1992.